IBIS/PICsIT Instrument Specific Software Scientific Validation Report

Luigi Foschini
INAF/IASF-Bologna, Italy

Version 5.1

December 7, 2005

Prepared by: L. Foschini (INAF/IASF-Bologna, Italy)

With contributions by:

G. Malaguti (INAF/IASF-Bologna, Italy)
A. Goldwurm, A. Gros, P. Laurent (Service d'Astrophysique, CEA-Saclay, France)
P. Lubinski, N. Produit (ISDC, Geneva, Switzerland)
L. Natalucci (INAF/IASF-Roma, Italy)
T. Mineo (INAF/IASF-Palermo, Italy)

Approved by:

P. Ubertini (IBIS PI)
G. Di Cocco (IBIS CoPI)

	Revision History
v 1.0	First version for first software release of March 2003.
28/02/2003	
v 1.1	Update for the intermediate software release of May 2003.
30/04/2003	Early analysis of Cyg X–1, cleaning of cosmic–ray induced events, improvement of the position accuracy, comparison with ECOE data.
v 1.2	Update for OSA 3 release.
27/10/2003	Crab in rev 102; automatic source location; timing analysis. Some error corrected. Removed the non–standard analysis section.
v 2.0	General reshape of the document style. Update for OSA 3.1 release.
02/02/2004	Updated the discussion on the uniformity maps and the inclusion of GTI.
v 4.0	Update for OSA 4 release (jump in the version number to match the OSA version).
06/07/2004	New executable for mosaic. New background maps.
v 5.0	Update for OSA 5 release. Revision of deconvolution algorithm.
28/07/2005	Module for spectra extraction.
v 5.1	Update for OSA 5.1 release.
07/12/2005	Background studies.

1 Introduction

This report summarizes the scientific performances and reliability of the Instrument Specific Software (ISSW) of the PICsIT detector layer of the IBIS imager aboard INTEGRAL (see Di Cocco et al. 2003 for more details on the instrument). The executables analysed here, together with their Instrument Configuration (IC) files, are those delivered by the IBIS Team to the ISDC for the integration in the Off–line Scientific Analysis (OSA) software package version 5.1 released by the ISDC to the public by 24 November 2005. An equivalent report on the IBIS/ISGRI ISSW is provided in a separate document by A. Goldwurm et al. (IBIS/ISGRI Instrument Specific Software Scientific Validation Report).

The basic concepts of the scientific analysis of the IBIS telescope are described in Goldwurm et al. (2001, 2003), while more detailed technical information about the pipelines, data structures, tools, and complementary modules can be found in the documents *Introduction to INTEGRAL Data Analysis* (ISDC/OSA–INTRO), *ISDC Data Repository Organization* (ISDC/TEC013), and *IBIS Analysis User Manual* (ISDC/OSA–UM–IBIS). Specific descriptions, performances, and problems of the pipeline scripts or other executables not provided by the IBIS Instrument Team (IT), as well as installation problems, operating systems compatibility, hardware load, and so on, are not analyzed and reported here.

This report provides a evaluation of the scientific performances of the IBIS/PICsIT software according to the tests performed so far. Further tests will be available in the next versions of the present document. We also underline that this document does not provide a comprehensive analysis and evaluation of the IBIS/PICsIT in-flight calibrations and instrument performances, although some results described in the present report can be used for that purpose.

2 The IBIS/PICsIT data analysis

2.1 General concepts

The general purpose in the data analysis of astronomical instruments can be basically divided into two parts: the first, based on the analysis of images, is to measure the celestial coordinates, the spatial structure (extended or point–like sources), and the photometry of the source. The second, related to the study of the spectra, is to measure the flux and energy of emission/absorption lines, and the characteristics of the continuum. The measuring process adds several effects that contribute to modify the original image or spectrum. Therefore, it is necessary to operate corrections to the data in order to obtain an image/spectrum that is as much as possible consistent with the original one. Despite the differences depending on the instrument used in the observation, from a purely conceptual point of view, it is necessary to solve an inverse problem with distribution functions. In other words, by assuming for the sake of simplicity a monodimensional case, we have to solve the following integral equation of Fredholm of the first kind:

$$\phi(x) = \int \psi(z) K(x,z) dz \tag{1}$$

where ϕ is the observed density of probability function, while ψ is the corresponding original density of probability fuction that we want to restore. K is the kernel of the integral equation and represents the measuring process, including the effects of the measuring errors in the observed distribution. The kernel is called *point–spread function* (PSF) in the images, while it is called *line–spread function* (LSF) in the spectra. ϕ, ψ, and K are all non–negative functions, since they are connected with the density of the incoming photons.

The basic problem of the astronomical software is therefore "to clean" the PSF or LSF from all the

systematic errors (including those of calibrations), before to proceed to the inversion of the integral equation. At the end of the correction ("cleaning") process, the kernel should contain only the statistical errors intrinsic to the measuring process. For example, in the case of a gaussian distribution with variance σ^2, the kernel is:

$$K(x,z) = \frac{1}{\sigma\sqrt{2\pi}} \exp \frac{-(x-z)^2}{2\sigma^2} \tag{2}$$

Depending on the type of instrument, there are different types of corrections. A system for astronomical data processing can be divided into three main steps, which in turn can be divided into sub–steps. The first step (**Level 0**) is the *preprocessing* level, where the telemetry coming from the satellite is unpacked and converted into a standard format (FITS) (see in the ISDC Technical Document section[1]). The basic data structure (RAW and PRP) is built, together with the On–Board Time (OBT) information, and the division into Science Windows (ScW) is set up (see ISDC/TEC013 for more details).

It is worth noting that, in the case of IBIS/PICsIT, there is also an on–board processing of the data before the Level 0, performed by the Hardware Event Preprocessor of IBIS (HEPI). This is necessary because of the limited telemetry available on–board the INTEGRAL satellite and the high count rate of background (≈ 3500 c/s) in the IBIS/PICsIT energy range ($0.17 - 10$ MeV). Therefore, HEPI performs a preliminary processing of the event list (containing the position y, z of the pixel, the channels $0 - 1023$, and the time information), before to send it to the ground. The corrections are: equalization by applying the gain and offset values of the HEPI look–up tables (LUT), conversion from channels to energy to reconstruct the multiple events, integration of events into histograms to save telemetry. The histograms are divided into two types: one (*spectral imaging*) is a data cube of $256 \times 64 \times 64$, containing still the full spatial information (64×64 pixel) and a moderate energy resolution (from the original 1024 to 256 channels). The integration time of a single histogram is generally corresponding to the duration of one ScW (≈ 2000 s), resulting in a loss of time information. Therefore, to perform time study, the other type of histogram (*spectral timing*) is designed to keep time resolution down to 1 ms, but with a great loss of energy resolution (from 1024 to 8 channels), and without spatial information. The combination of the *spectral imaging* and *spectral timing* is called *standard mode*. It is worth noting that IBIS/PICsIT can download directly the event list, without the integration on–board (*photon–by–photon* mode PPM), but with great consumption of telemetry. Therefore, with the exception of some observations of calibration, IBIS/PICsIT works only in standard mode, by producing spectral imaging histograms for single and multiple events, and histograms in spectral timing (default 4 energy bands and 4 ms of time resolution). More details on IBIS/PICsIT on–board processing are available in the IBIS User Manual, Issue 5.1.

Once the basic data structure is set up, there is the correction step (**Level 1**) where the instrument dependent corrections are applied. In this level, the OSA pipeline starts to work and perform the sublevels COR, DEAD, GTI, BIN_I/BIN_S, BKG_I/BKG_S. The specific corrections for IBIS/PICsIT are:

1. the intrinsic deadtime of the detector, that is the time during which it is not possible to process any event, since the detector is devoted to the processing of another event;
2. additional deviations from the on–board tables of gain and offset (only for PPM), and conversion from channels to energy;
3. filtering of the events according to the Good Time Intervals (GTI); for PPM only;
4. correction of partially downloaded histograms (for standard mode only);
5. correction for detector non–uniformities and subtraction of the background.

[1] Available at `http://isdc.unige.ch/index.cgi?Documents+doctec`.

When the data are cleaned from background and corrected for instrumental effects, it is possible to move to the third level (**Level 2**), where the creation of images, spectra, and lightcurves is done (sublevels CAT_I/CAT_S, IMA/IMA2, SPE, LCR). The shadowgrams, produced in the previous level, are deconvolved according to the algorithms explained in Goldwurm et al. (2001, 2003), and the search for known sources is done, starting from a general catalog (Ebisawa et al. 2003). The attitude values of right ascension and declination obtained from the star tracker are referred to IBIS/PICsIT, by using a rotation and traslation (IBIS/PICsIT and the star tracker are not aligned). Moreover, the deconvolved image is projected into the sky with the gnomonic projection (TAN, cf Calabretta & Greisen 2002). The standard products of the source detection, performed on the sky images, is composed of the source coordinates and errors (in celestial coordinates and in pixels), the flux and its error (in counts per second), and the significance.

In the part of the extraction of the spectra, whose algorithms are still described in the seminal papers by Goldwurm et al. (2001, 2003), two IC files are of extreme importance. The first, named Auxiliary (or Ancillary) Response File (ARF) contains the information about the effective area of the detector as a function of the photon energy. The second IC file is named Redistribution Matrix File (RMF) and contains the information necessary to convert the counts into photons. A full description of the IBIS RMF/ARF is presented in Laurent et al. (2003).

The lightcurves are generated by using the spectral timing data, and therefore they are simply the count rates versus time for the whole detector. The deadtime and barycentric corrections are applied. The extraction of lightcurves for single point sources is not yet implemented, since it can be done only in PPM.

The output of the OSA pipeline can be analysed by means of the common software for high–energy astrophysics (e.g. `xspec`, `ds9`, `xronos`, ...).

2.2 General description of the executables

The IBIS/PICsIT–ISSW delivered to date for the Scientific Analysis of the PICsIT data include:

- `ibis_pics_deadtime` (v 2.4.1, 31 May 2004, DEAD level):
  to calculate the intrinsic deadtime of each semimodule of the detector. It is based on the use of a specific IBIS/PICsIT housekeeping, the *livetime counter*, that provides already the effective live time for each semimodule every 8 seconds. It provides also a display for the temperatures of each module.
- `ip_ev_correction` (v 1.8, 6 September 2005, COR level):
  to perform a correction of gain and offset variations in addition to those performed on board by HEPI. It is only for data obtained in photon–by–photon mode. It is strictly linked with the IC data structure `PICS-ENER-MOD`, containing the average gain, offset, and the deviations, pixel by pixel, from these values. Presently, no deviations are implemented, that is, only the onboard equalization are used. See Malaguti et al. (2003) for details on in-flight gain/offset behaviour.
- `ip_ev_shadow_build` (v 2.6, 2 June 2005, BIN_I/BIN_S level):
  to perform the building of the shadowgrams and the efficiency maps (dimensions 64×64) from data in photon–by–photon mode, according to energy bands or time bins selected by the user. The events are cleaned from the spurious events induced by cosmic-rays or noisy pixels (see Sect. 5 for more details) and selected according to the available table of Good Time Intervals (GTI), which in turn are generated by another set of executables made by ISDC.
- `ip_si_shadow_build` (v 3.1.3, 4 June 2005, BIN_I/BIN_S level):
  to perform the building of shadowgrams and the efficiency maps (dimensions 64×64) from

the dat in standard mode (spectral imaging). It reads the binning tables from the IC file `PICS-BINT-CFG` (containing the data of the onboard HEPI LUT) and converts into channels the requested energy bands. By default, if histograms are not complete, the executable returns simply a warning, but it continues the analysis by discarding it. If the user wants to correct and use also partially downloaded histograms, it is possible to set the threshold below which the executable correct (the missing pixels will be trated as killed pixels) and integrate the partially downloaded histograms. The parameter to set is `IBIS_IPS_corrPDH`, that has to be put equal to the maximum number of allowed missing cells. It is better to keep `IBIS_IPS_corrPDH`$\leq$ 10000. In `rev_2` data type, it is possible to discard also those shadowgrams affected by problems in resynchronization of HEPI (see `IA19` and `SCREW1406`).

- `ip_shadow_ubc` (v 3.1, 24 March 2004, BKG_I/BKG_S level):
to perform the correction for background and detector non–uniformities. The output shadowgrams are also expanded to take into account the gaps between modules (from 64×64 to 65×67). The gaps and the killed pixels are filled with a mean value of counts averaged over the whole detector. There is also a variance map, calculated starting from the statistical variance of the detector counts and updated according to the correction performed (filled pixels, background subtraction, and so on...). The executable is linked with the following IC data structures: `PICS-SBAC-BKG` (background maps for single events), `PICS-MBAC-BKG` (background maps for multiple events), `PICS-SUNI-BKG` (detector non–uniformities for single events), and `PICS-MUNI-BKG` (detector non–uniformities for multiple events). See Sect. 3 and 4 for details.

- `ip_skyimage` (v 3.2, 7 September 2005, IMA2 level):
it performs the deconvolution and sky image reconstruction by means of the algorithm described by Goldwurm et al. (2003). The executable provides a basic deconvolved sky image, significance, and variance maps. The latter are optional and the default is no variance maps in output (`PICSIT_outVarian=0`). The sky projection adopted is the gnomonic one (`TAN`[2]). It is also possible to use as input a set of variance shadowgrams already corrected for the background subtraction: in this case, the significances in output should be read as values already corrected for the background. This was the default option with previous releases of OSA: starting from OSA5, the default option will be to use the variance shadowgram not corrected, but there is the opportunity to return to the old way by setting the parameter `PICSIT_inCorVar=1`. For staring observation, it is possible to integrate the shadowgrams before the deconvolution and the automatic source location. For observations with dithering pattern, it is not possible to sum the shadowgrams before the deconvolution. Therefore, this module perform the basic deconvolution for every ScW. The weighted integration of the ScW images (mosaic) is the task of next executable.

- `ip_skymosaic` (v 1.6.1, 5 October 2005, CLEAN level):
it performs the integration of the individual ScW images into a single image (mosaic). It works mainly for dithering observations, but it can be used for staring pointings as well. It performs an integration with linear interpolation of the pixels, weight with the significance, and automatic source detection. The default sky projection is the gnomonic one (`TAN`), but it is possible also to change to stereographic (`STG`) or zenithal equidistant (`ARC`), the latter useful for polar regions. It is worth noting that PICsIT data work fine also with the `varmosaic` tool by K. Ebisawa provided by `HEASoft v. 6.0`: in this case, it is necessary that the OSA produce sky images per Scw with variance maps (i.e., set `PICSIT_outVarian=1`). Please note that `ip_skymosaic` works instead with `PICSIT_outVarian=0`, that is no variance maps in output[3].

- `ip_st_lc_extract` (v 2.4, 3 March 2005, LCR level):
it performs the extraction of the lightcurve of the whole detector from the spectral timing data. In the case of overflow error, the lightcurve is truncated to the latest useful value and

[2]For more information of sky projections, see Calabretta & Greisen (2002).

[3]This bug has been already corrected in the v 1.7, delivered to ISDC on 16 November 2005, but too late to be included in the OSA 5.1 release.

an error message is written in the log file. The barycentric correction is not applied, and the output should be processed with the OSA tool `barycent`.

- `ip_spectra_extract` (v 2.2, 12 September 2005, SPE level):
  it performs the extraction of the spectrum of point sources from data in any mode (both photon-by-photon and standard), by using the Pixel Illumination Factor (PIF). Given the few sources detected (and expected) in the PICsIT energy range, the executable works for one single source. In this way, it is possible to make a simplified version of the algorithm described in Goldwurm et al. (2003). The energy bands are selected from the `RMF` file, that therefore should be rebinned according to the user's preferences before to run the pipeline.

It is worth noting that the OSA for IBIS/PICsIT makes use of other executables in addition to those described above (creation and merging of GTI, Catalog Extraction, and so on...). These executables have been developed by ISDC people (N. Produit, R. Rolhfs, L. Lerusse) and are not analysed here directly, although the proper working of these modules is essential to have the full software package. These executables work well to date.

3 Maps for Background Correction

IBIS/PICsIT operates in an energy region dominated by the background (that is also higher than expected from numerical models – cf Ferguson et al. 2003), where we expect that the source counts are of the order of a few percent of the global counts detected. This means that the background correction is of paramount importance for the instrument capabilities.

The photons interacting with IBIS/PICsIT are distributed in a non–uniform way, because of several reasons (see Natalucci et al. 2003 for more details). The main effect is to produce an enhancement of counts at the edges of the modules and semimodules. Therefore, before to perform the deconvolution, it is necessary to flatten the detector non-uniformities and to correct for the background. For this purpose, it is possible to use shadowgrams built from empty field observations, but it is also possible to integrate a long number of Scw also from pointed observations, because in the energy range of PICsIT ($0.2-10$ MeV) there are a few sources. Moreover, since *INTEGRAL* is operating mostly in dithering mode, this means that by summing all the shadowgrams pixel by pixel, any possible contribution of sources is blurred.

3.1 Single events background

In the following, the background behaviour of single events only is discussed. All public data, from observations of GPS, GCDE, Crab and Vela Region, available on 6 June 2004 were used. There are 85 shadowgrams for single revolutions and 6 shadowgrams for longer exposures, gathering data from 4 up to 19 revolutions. Revolutions 0031 and 0166 were not taken into account because there are only 1 and 3 scws processed, respectively. Also revolution 0168 is not used due to some problems with processing the consolidated data. The only criterion to exclude PICsIT single event histograms from including it in the shadowgram were missing cells. Shadowgrams were prepared with the OSA 4. The list of all studied revolutions is presented in Tables 1 and 2, where also exposures and average count rates obtained for an entire shadowgram in 8 new energy ranges are listed.

3.2 Count rate histograms

Figures 1 and 2 show the distribution of count rates measured for single pixels in two long exposure shadowgrams from years 2003 and 2004, respectively. Histograms of count rates are plotted for eight

Table 1: Total count rates for shadowgrams collected in 8 energy ranges: 1 (203 – 252 keV), 2 (252 – 336 keV), 3 (336 – 448 keV), 4 (448 – 672 keV), 5 (672 – 1036 keV), 6 (1036 – 1848 keV), 7 (1848 – 3584 keV), 8 (3584 – 6720).

Rev.	Scws	Exposure	Counts per second								Comment
		[ks]	(1)	(2)	(3)	(4)	(5)	(6)	(7)	(8)	
0036	7	15.3	629	482	308	351	211	167	63	24	GPS
0038	4	12.9	653	498	320	368	226	182	71	28	Empty Field
0039	24	96.8	655	493	317	369	229	185	73	28	Crab
0043	63	176	563	427	275	320	199	159	62	24	Crab
0044	69	150	631	473	304	354	219	176	69	27	Crab
0046	5	10.9	640	470	305	360	228	185	75	30	GPS,GCDE
0047	82	150	644	479	310	361	225	182	72	28	GPS,GCDE
0049	38	67.7	644	474	307	360	226	182	73	28	GCDE
0050	64	131	640	474	306	359	224	181	72	28	GPS,GCDE
0051	57	113	645	482	311	362	224	180	70	27	GCDE,GPS
0052	16	29.3	651	476	310	361	228	184	76	30	GCDE
0053	61	110	636	474	305	354	219	176	68	26	GCDE
0054	68	128	653	482	311	364	227	184	73	28	GPS,GCDE
0055	29	64.1	643	482	311	361	223	179	70	27	GPS,GCDE
0056	56	102	639	471	305	356	222	179	71	28	GCDE
0057	40	84.4	644	478	308	360	224	181	71	28	GCDE
0058	15	31.9	642	480	309	359	222	178	70	27	GPS
0059	58	71.6	651	480	310	361	225	181	72	28	GPS,GCDE
0060	16	29.3	628	466	301	349	216	172	67	26	GCDE
0061	37	66.3	637	472	304	353	218	175	68	26	GCDE
0062	67	142	638	471	304	355	221	178	70	27	GPS,GCDE
0063	41	78.8	641	469	303	354	222	179	71	28	GPS,GCDE
0064	82	145	654	487	314	364	224	180	70	27	GCDE
0065	66	118	646	480	309	358	220	176	69	27	GCDE
0066	76	143	628	463	299	348	216	174	68	27	GPS,GCDE
0067	12	26.0	632	470	302	350	215	172	67	26	GPS
0070	11	24.0	631	463	299	349	218	175	69	27	GPS
0071	9	19.6	638	469	302	352	220	177	70	27	GPS
0074	11	24.0	657	484	311	363	225	182	72	28	GPS
0076	13	28.7	663	535	353	406	241	197	92	39	GPS
0078	12	26.2	634	466	300	348	216	173	68	26	GPS
0079	12	27.6	631	465	299	348	216	173	68	26	GPS
0082	57	169	627	469	302	351	218	175	70	27	GPS
0083	63	193	619	465	300	350	218	176	72	29	GPS
0086	66	204	594	437	282	330	208	168	67	27	GPS
0087	63	192	608	448	291	341	216	175	71	28	GPS
0091	7	15.2	655	495	315	355	211	166	62	23	GPS
0092	7	15.2	587	440	280	318	191	151	57	21	GPS
0096	19	35.2	642	457	296	348	222	179	73	29	Empty Field
0097	7	11.9	642	471	303	350	217	173	68	26	GCDE
0100	108	186	656	479	308	356	219	175	68	26	GCDE
0101	9	15.9	667	485	312	361	223	178	69	27	GCDE
0102	9	36.2	662	465	302	356	228	185	77	31	Crab
0103	95	163	650	467	302	353	222	178	72	28	GCDE

Table 2: Total count rates for shadowgrams collected in 8 energy ranges: 1 (203 – 252 keV), 2 (252 – 336 keV), 3 (336 – 448 keV), 4 (448 – 672 keV), 5 (672 – 1036 keV), 6 (1036 – 1848 keV), 7 (1848 – 3584 keV), 8 (3584 – 6720).

Rev.	Scws	Exposure	Counts per second								Comment
		[ks]	(1)	(2)	(3)	(4)	(5)	(6)	(7)	(8)	
0115	5	7.1	693	504	325	376	233	187	74	29	GCDE
0116	90	160	692	496	321	376	236	190	77	30	GCDE
0117	102	192	693	499	322	376	236	190	76	30	GCDE
0118	97	175	697	494	321	378	239	194	79	31	GCDE
0119	107	190	691	486	316	373	238	193	79	32	GCDE
0120	101	179	681	477	311	367	234	189	78	31	GCDE
0121	103	184	681	479	312	368	234	190	78	31	GCDE
0122	102	183	691	487	317	374	238	193	80	32	GCDE
0123	88	153	694	490	319	376	239	193	79	32	GCDE
0130	61	176	917	833	572	661	387	224	82	32	Empty Field
0137	99	178	620	455	301	356	223	164	62	24	Vela
0138	103	186	649	484	319	376	232	176	70	27	Vela
0139	91	160	654	483	316	370	228	174	68	26	Vela
0140	98	170	657	481	313	366	227	174	66	26	Vela
0141	95	175	651	476	310	361	224	172	66	25	Vela
0142	10	22.7	621	455	296	345	215	166	64	25	GPS
0145	11	25.4	675	493	319	372	232	182	71	28	GPS
0146	10	21.8	670	488	316	368	229	180	70	27	GPS
0149	9	19.5	689	501	324	377	235	186	73	28	GPS
0153	10	23.6	652	459	299	355	227	182	75	30	GPS
0154	16	42.4	653	455	297	353	226	183	75	30	GPS
0157	15	31.7	634	446	291	345	220	175	72	29	GPS
0161	12	26.2	676	462	302	360	233	189	79	33	GPS
0162	18	37.5	678	486	315	371	235	188	76	30	GPS
0163	27	48.5	682	502	324	372	230	182	72	28	GCDE
0164	77	140	705	497	324	383	243	196	80	32	GCDE
0165	101	189	708	495	323	383	244	198	81	33	GPS,GCDE
0167	99	188	708	508	329	387	243	194	77	30	GCDE
0169	103	187	705	496	323	382	243	196	80	32	GCDE
0170	14	32.4	707	514	349	380	238	192	75	33	GPS
0170	86	144	698	501	340	372	234	189	74	33	Crab
0171	89	158	719	514	350	384	242	196	77	35	GCDE
0172	72	128	707	499	341	375	238	193	77	35	GCDE
0173	13	23.0	719	513	350	384	242	196	78	35	GCDE
0174	106	191	720	515	351	384	242	196	77	35	GCDE
0175	35	64.3	725	513	351	386	244	198	79	36	GCDE
0177	28	69.4	684	495	337	369	232	188	74	33	GPS
0179	22	45.0	737	531	361	394	247	199	78	35	GCDE
0181	37	79.2	725	519	354	389	245	199	79	36	GPS,GCDE
0183	109	197	744	535	364	398	250	202	80	36	GCDE
0185	98	187	761	536	367	405	257	209	84	38	GPS,GCDE
long	880	1681	642	476	307	358	222	179	70	27	GPS,GCDE
sp03	331	939	617	459	297	345	216	174	70	28	GPS
su03	215	382	654	474	305	355	220	177	70	27	GCDE
au03	795	1432	689	488	317	373	236	191	78	31	GCDE
ja04	81	187	654	467	304	357	226	179	71	28	GPS
wi04	769	1420	708	503	334	382	241	194	78	32	GPS,GCDE

default PICsIT energy ranges, for entire detector area and for pixels lying on the edges of modules (rows 1, 16, 17, 32, 33, 48, 49, 64 and/or columns 1, 16, 17, 32). There is a clear change in the histogram shape observed for different energy bands. Usually the histograms for border pixels exhibit lack of low rate and excess of high rate cells.

3.3 Statistical results

Since it is impossible to plot such histograms for all revolutions and to have a more quantitative comparison between count rate histograms for various shadowgrams we have calculated some basic statistical parameters for these distributions. Figures 3-10 illustrate the evolution of the mean, standard deviation, median, skewness and kurtosis computed for all single revolutions, long exposure maps and Crab observations. For mean values we also present the pure statistical Poisson error of the total count number, divided by the exposure, which can be compared with the standard deviation obtained for histograms. The results for revolution 130 (i.e. that after the solar flare in Rev. 128) are not shown there since they differ strongly from the rest and then the differences between the other, "normal" revolutions are less visible. Besides the changes of the mean count rate and the distribution shape from revolution to revolution also a rather clear long term trend is visible. Particularly, after revolution 140 mean count rate is almost monotonically increasing.

3.4 "Nervous" pixels

In all shadowgrams there is a fraction of pixels showing a substantially higher (or lower) count rate than the mean. Such "nervous" pixels were localized with a criterion of deviation larger than three standard deviation from the mean derived for a given histogram. Figures 13-16 present the positions of these pixels on the detector plane, with four ranges of the frequency with which they appear in the data. Distribution of "nervous" pixels is energy dependent, however, for higher energies there are some structures repeated in all plots.

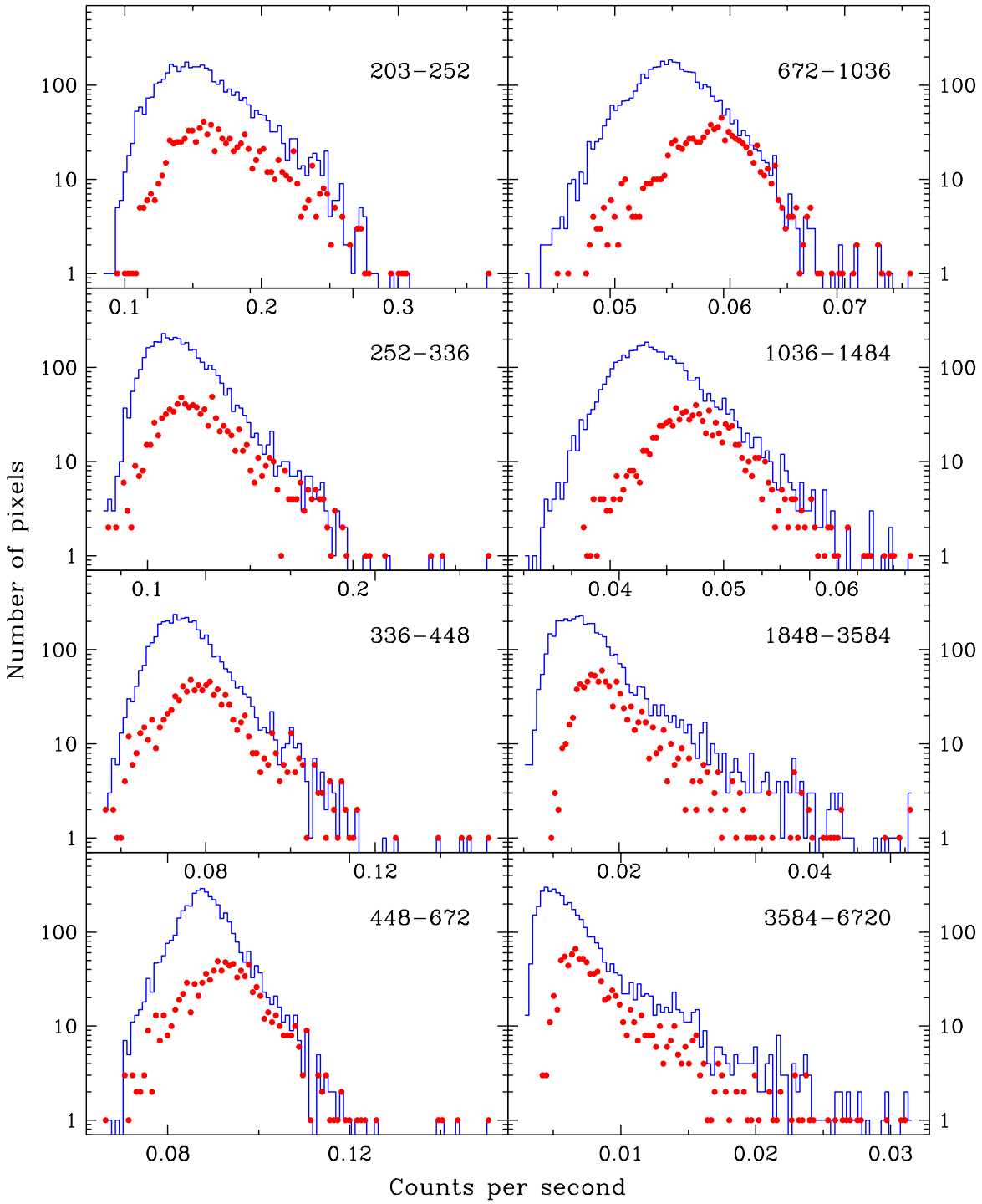

Figure 1: Count rate histograms for PICsIT pixels in eight default energy ranges. GPS and GCDE data from revolutions 0049 – 0067 (March-May 2003, map "long"), with 1681 ks exposure. Red dots show histograms for pixels lying on the modules edges.

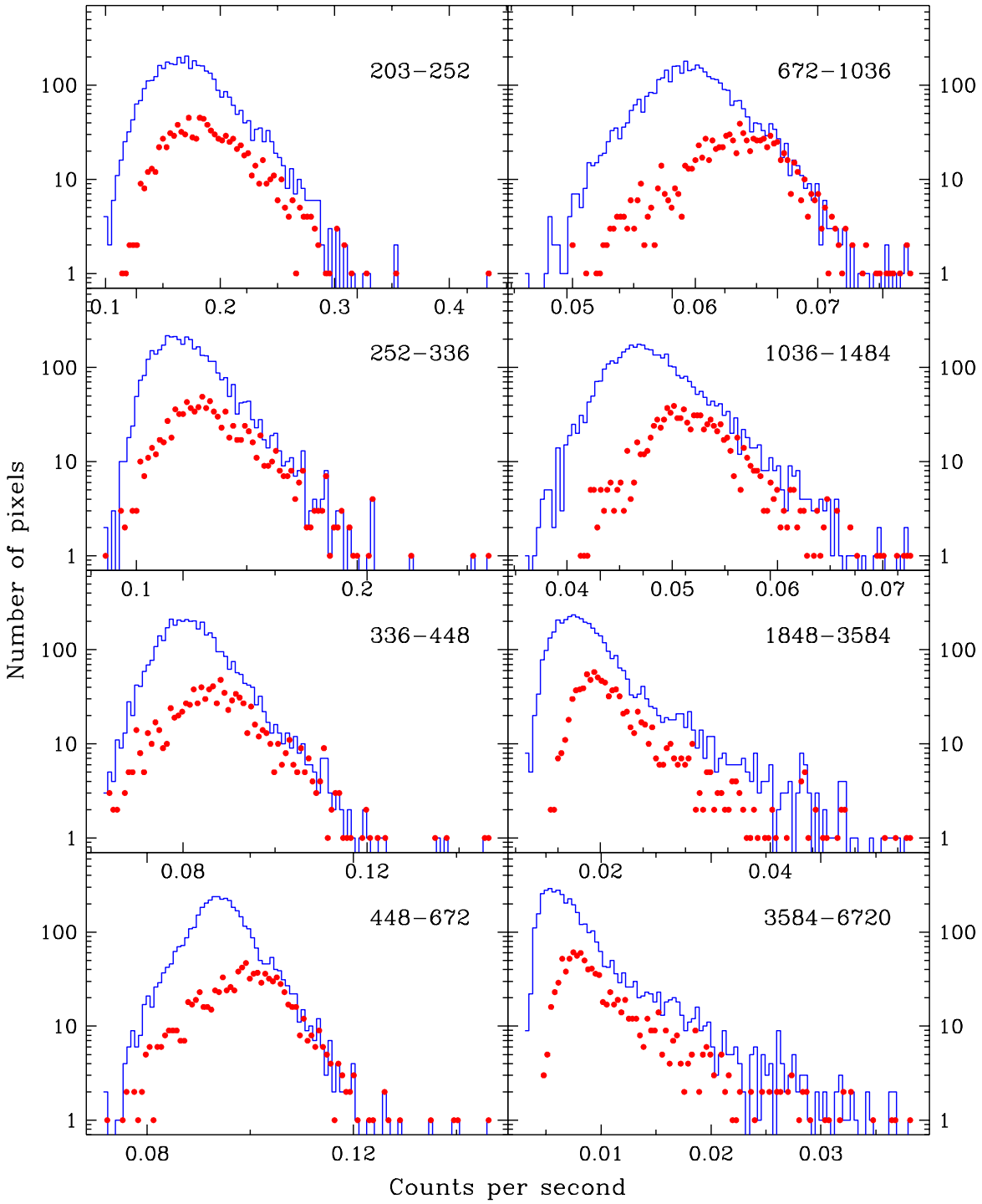

Figure 2: Count rate histograms for PICsIT pixels in eight default energy ranges. GPS and GCDE data from revolutions 0161 − 0175 (February-March 2004, map "wi04"), with 1420 ks exposure. Red dots show histograms for pixels lying on the modules edges.

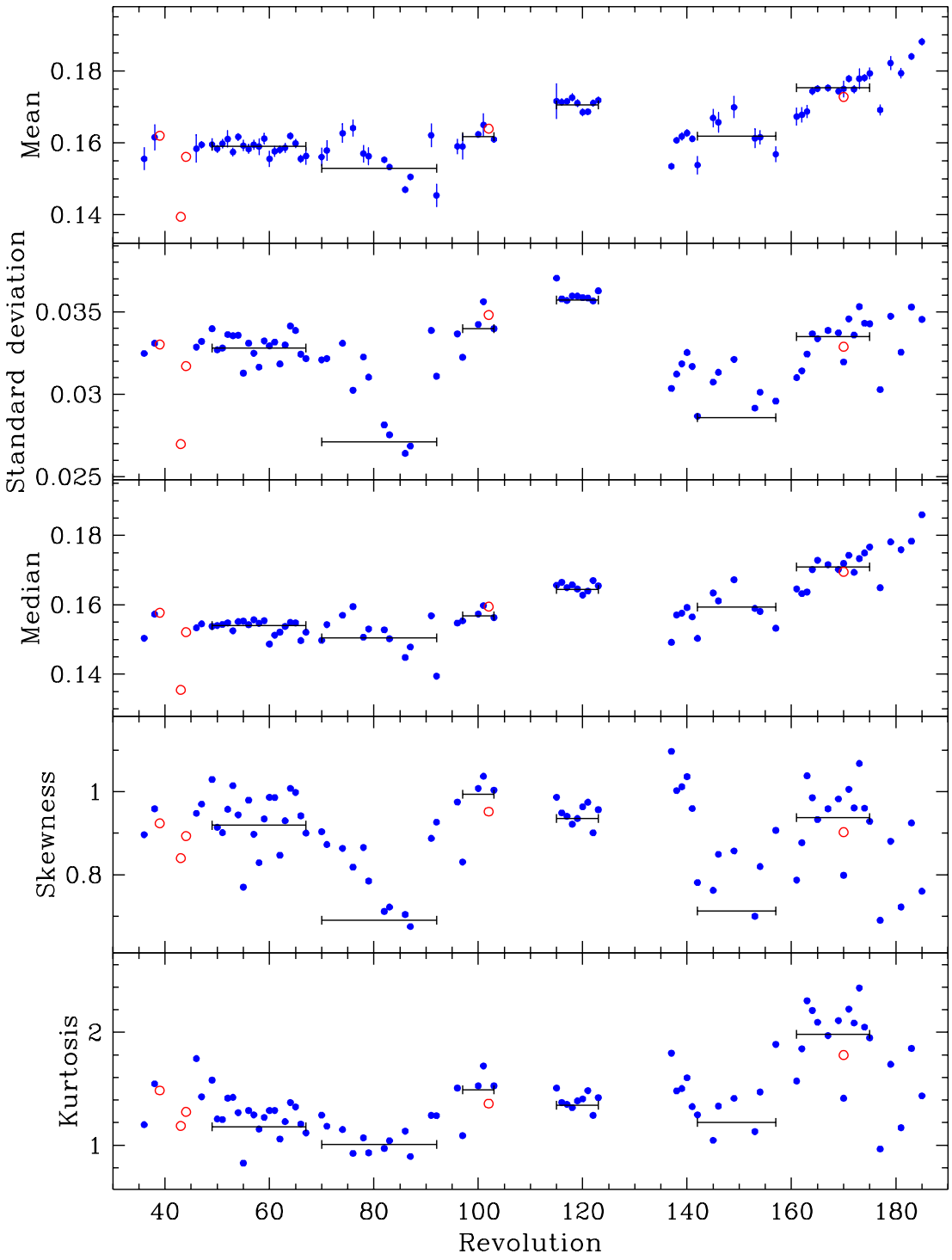

Figure 3: Statistical parameters obtained for PICsIT shadowgrams from different revolutions. Error bars for mean show the its Poisson uncertainty. Data for long exposure maps are shown with lines, Crab observation results are presented with open circles. Shadowgrams for entire detector and $203 - 252$ keV energy range were used.

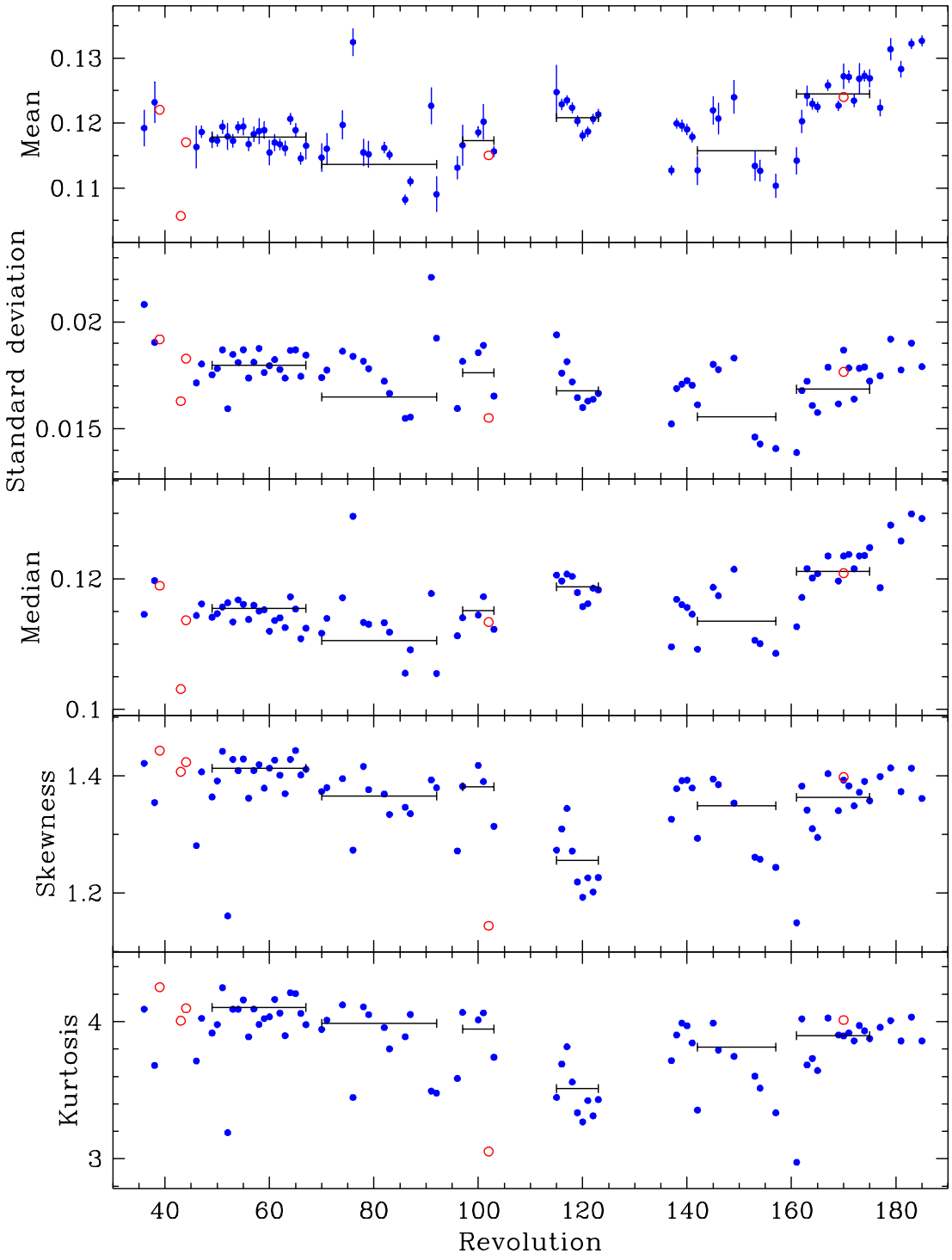

Figure 4: Statistical parameters obtained for 252 – 336 keV energy range.

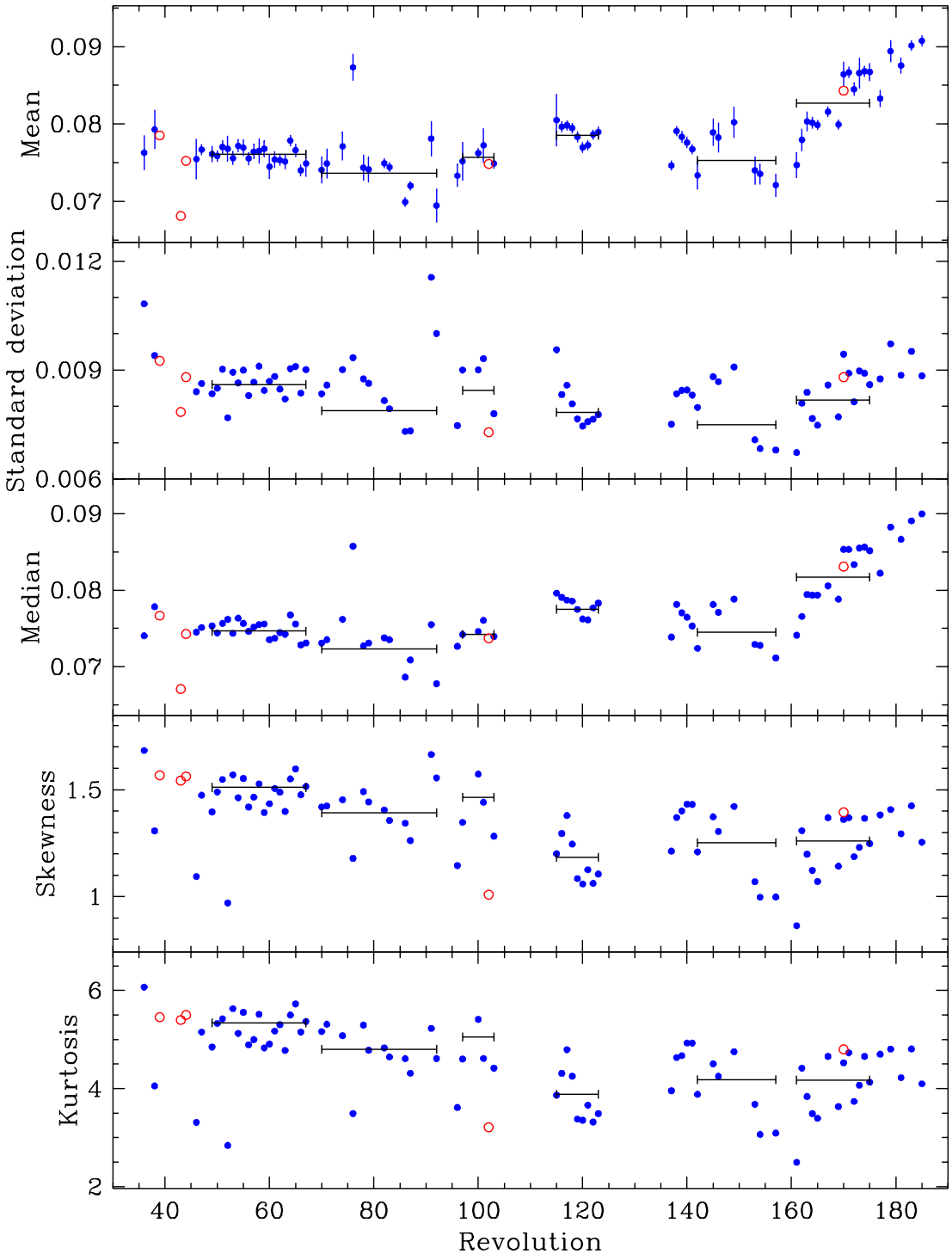

Figure 5: Statistical parameters obtained for 336 – 448 keV energy range.

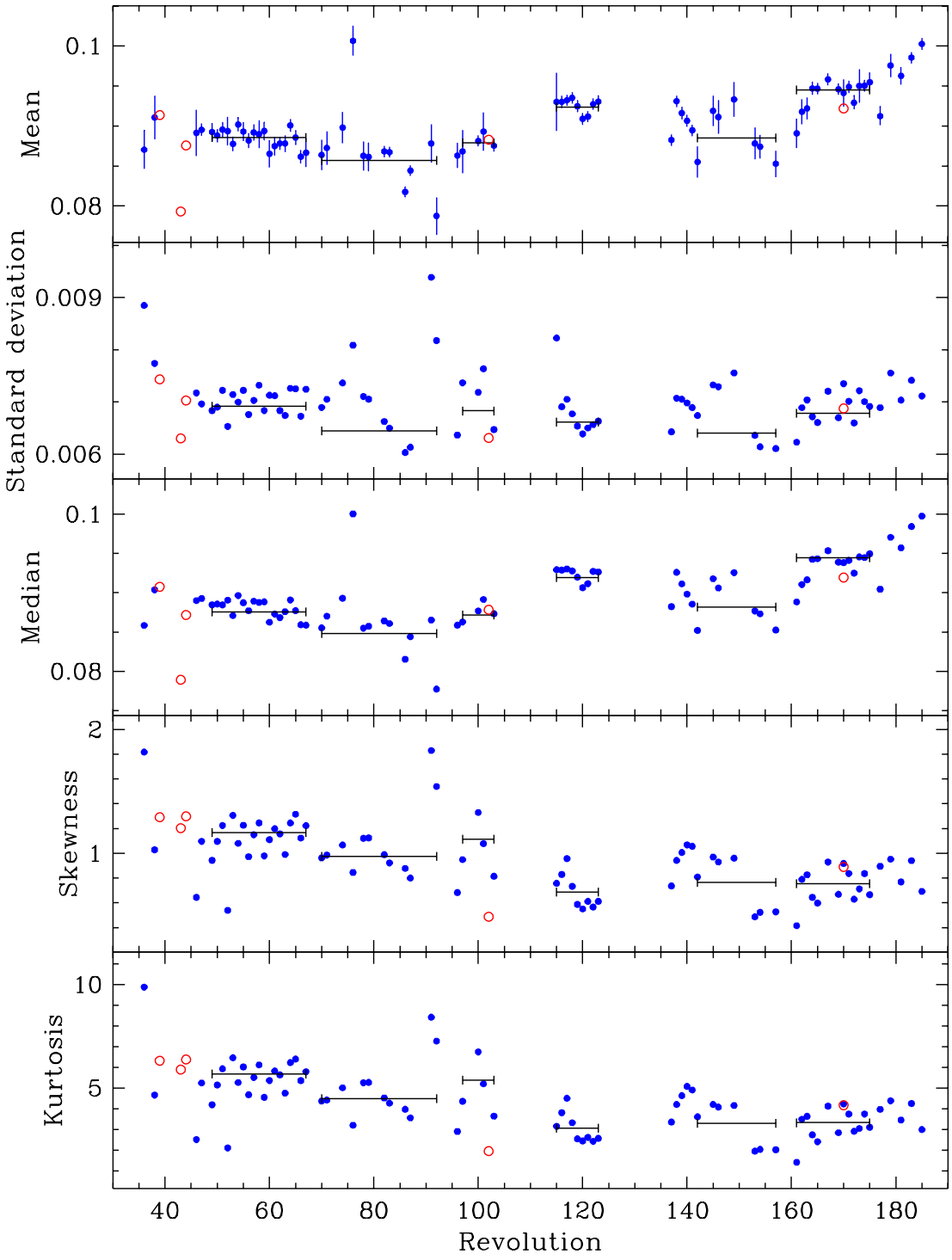

Figure 6: Statistical parameters obtained for 448 – 672 keV energy range.

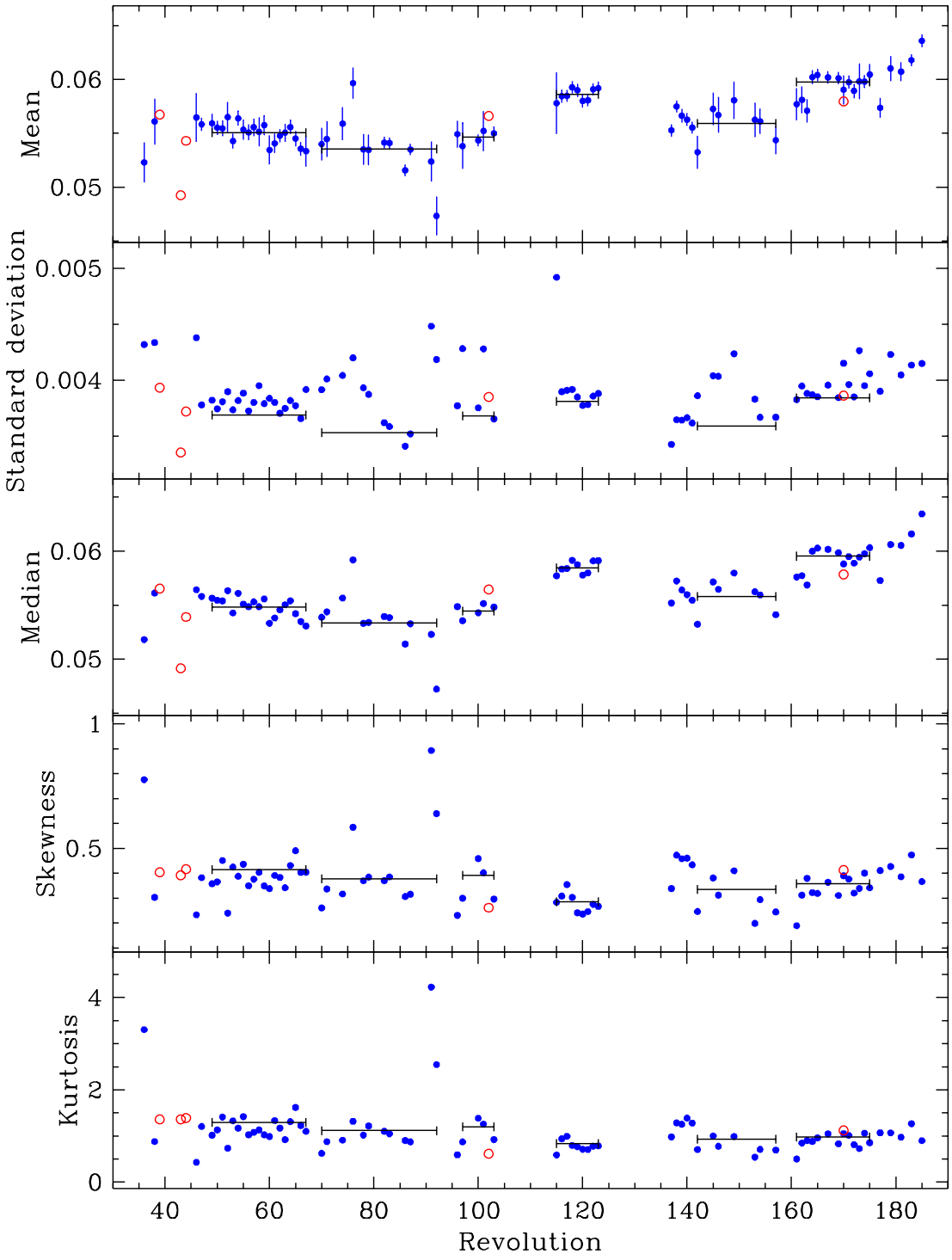

Figure 7: Statistical parameters obtained for 672 – 1036 keV energy range.

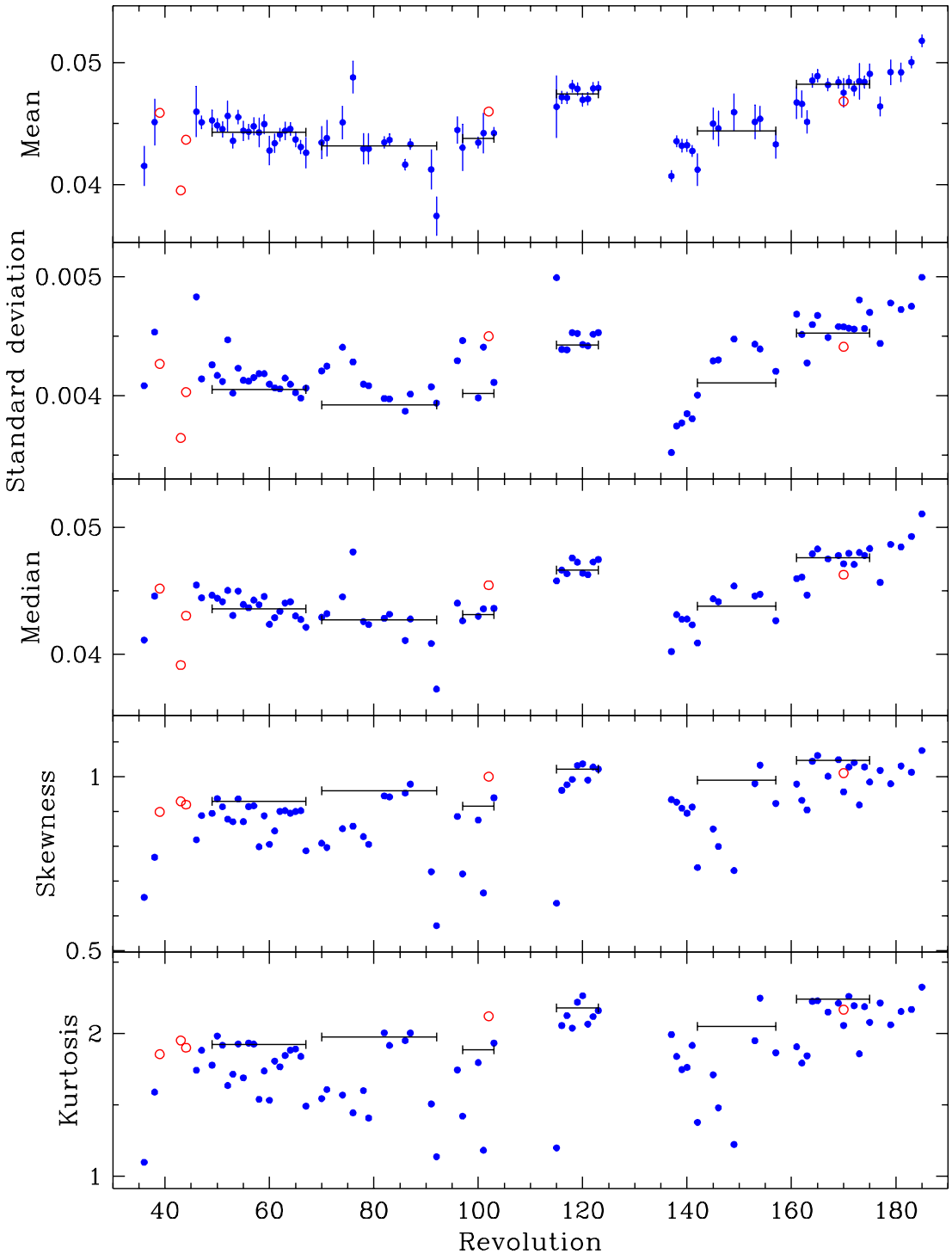

Figure 8: Statistical parameters obtained for 1036 – 1848 keV energy range.

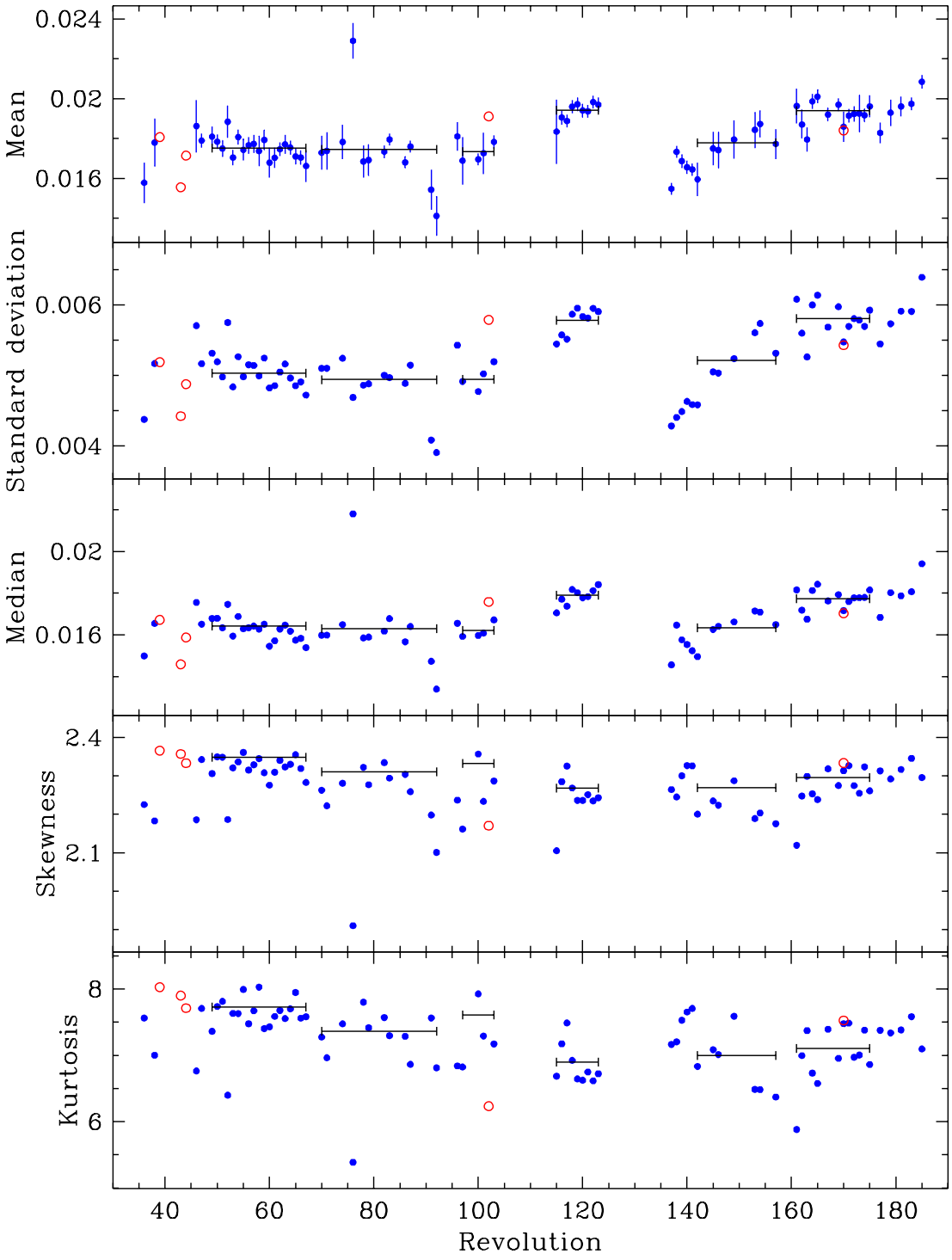

Figure 9: Statistical parameters obtained for 1848 – 3564 keV energy range.

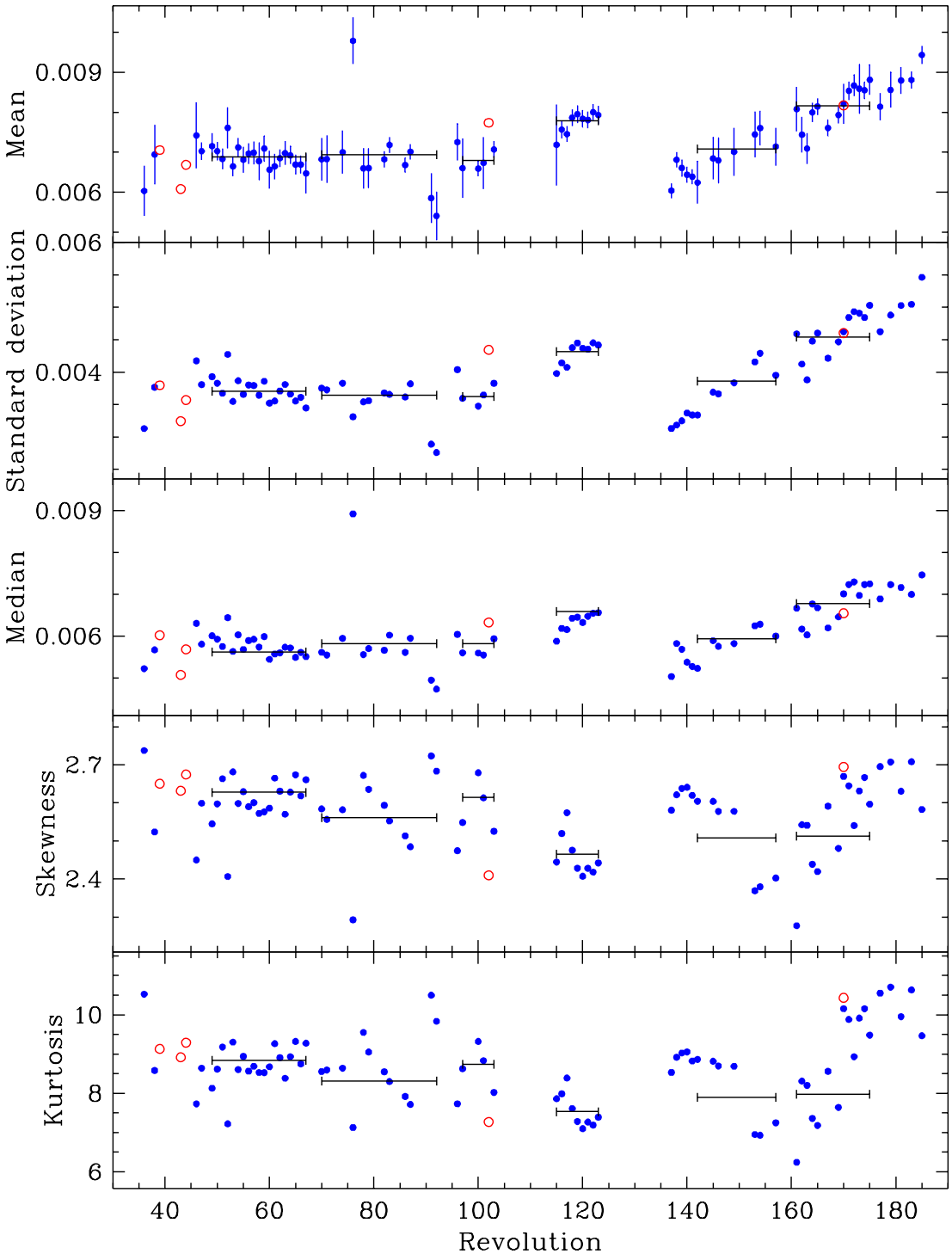

Figure 10: Statistical parameters obtained for 3564 – 6720 keV energy range.

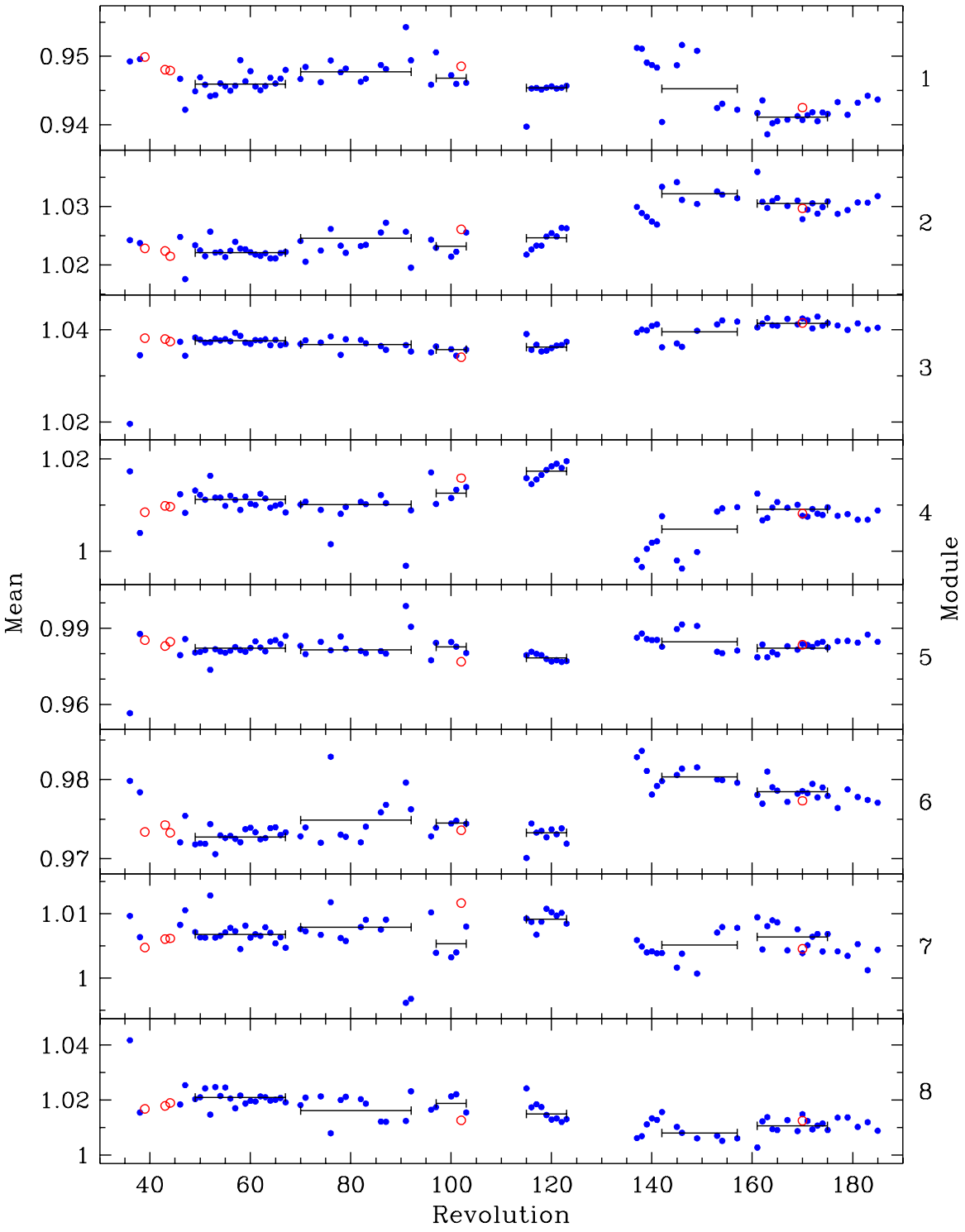

Figure 11: Ratios between mean obtained for different modules and mean obtained for entire detector. Energy range: 252 – 336 keV.

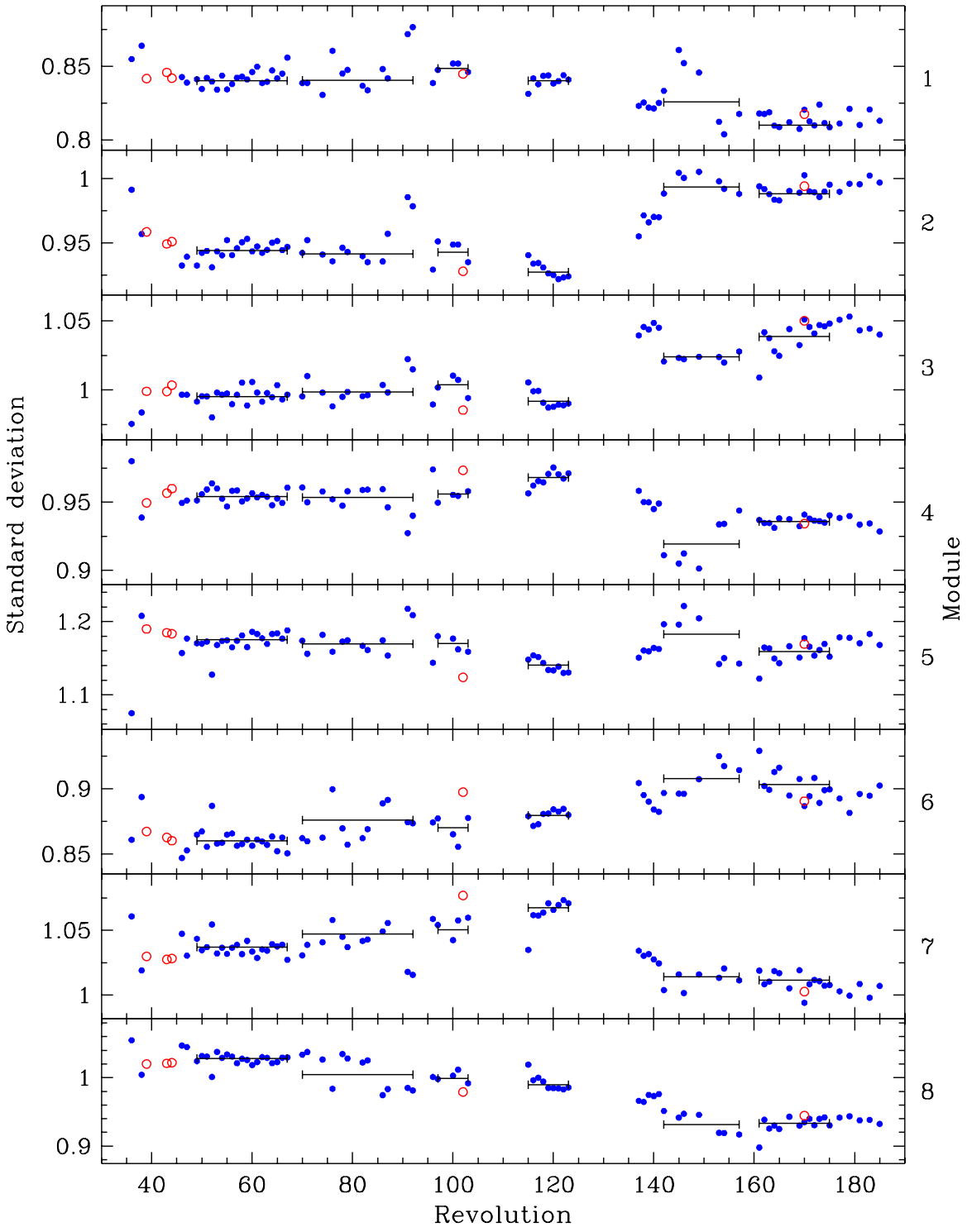

Figure 12: Ratios between standard deviation obtained for different modules and standard deviation obtained for entire detector. Energy range: $252 - 336$ keV.

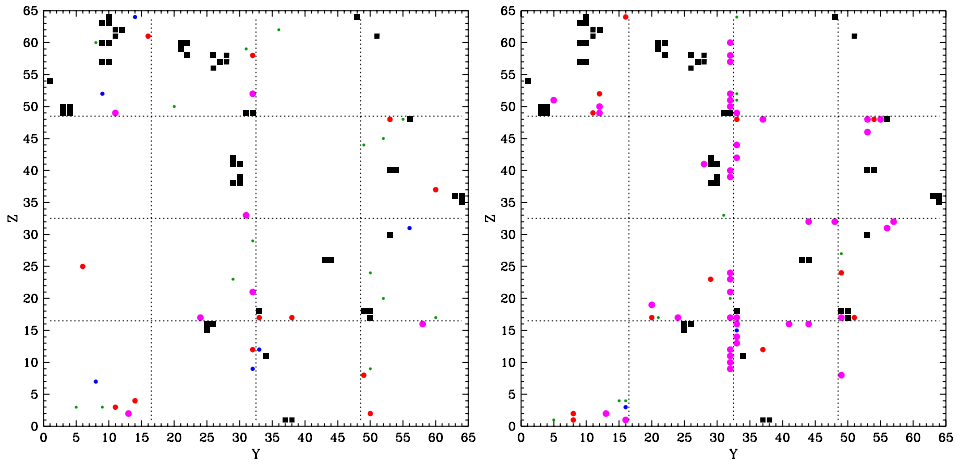

Figure 13: Distribution of "nervous" pixels on the detector plane. Killed pixels are shown with black squares. Pixels exhibiting higher than 3 σ deviation from the mean for more than 95% of revolutions are presented with the largest, magenta dots. Those with at least 70%, 50% and 30% occurence are shown with red, blue and green dots, respectively. Submodules borders are plotted with dotted lines. Left: results for $203 - 252$ keV, right: $252 - 336$ keV.

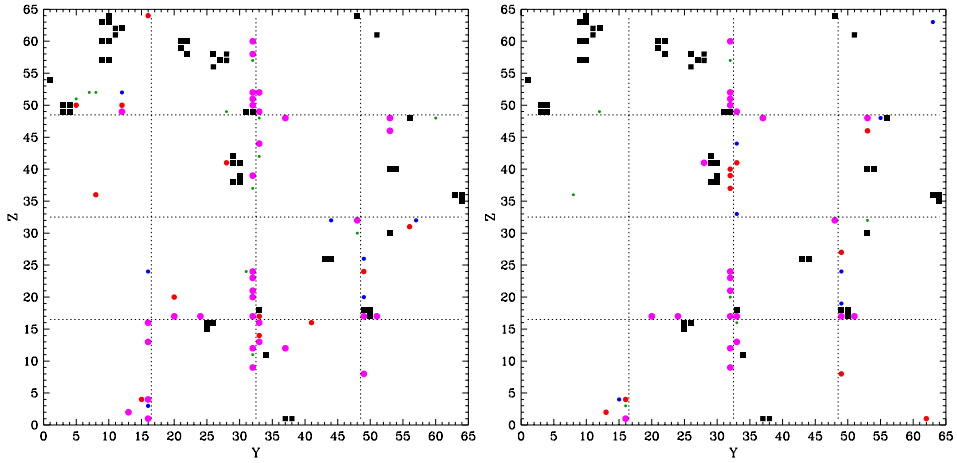

Figure 14: Distribution of "nervous" pixels on the detector plane. Left: results for $336 - 448$ keV, right: $448 - 672$ keV.

3.5 Shadowgrams comparison

As shown in previous subsections PICsIT background is variable on long time scale, with respect to its main characteristics, namely average count rate and spatial distribution of counts over the detector area. Therefore, a choice of data set for background map preparation should follow some criteria based on the study of this variability. Since there are only few observations of empty fields, the background maps relevant for sources observed in different times should be prepared with the data collected in dithering mode for sky regions having no strong sources. In this way also the uncertainty of the background will be reduced when there are many shadowgrams summed in one map.

Comparison between statistical parameters obtained for shadowgram with the interesting object with the parameters derived for various background shadowgrams may be used as a first step in background map selection. However, in histograms presented in previous sections the information on the pixel position is lost. Thus it is better to prepare for this purpose a another set of histograms, showing the distribution

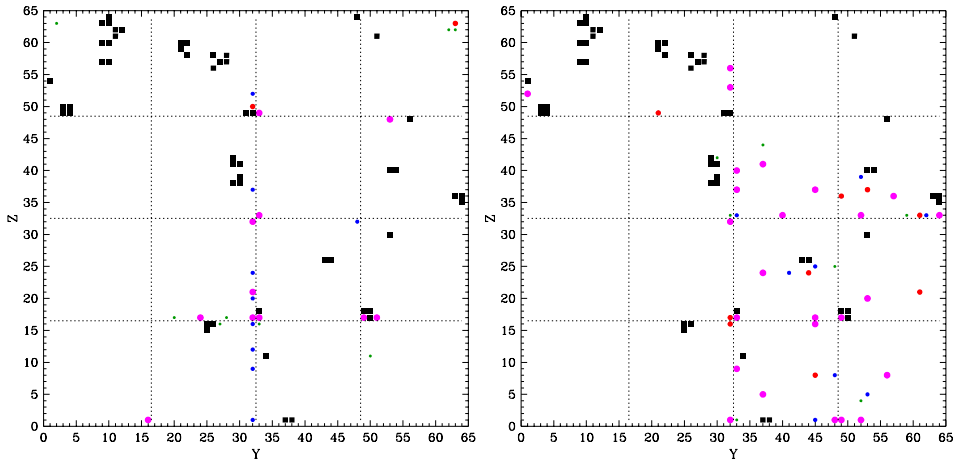

Figure 15: Distribution of "nervous" pixels on the detector plane. Left: results for $672 - 1036$ keV, right: $1036 - 1848$ keV.

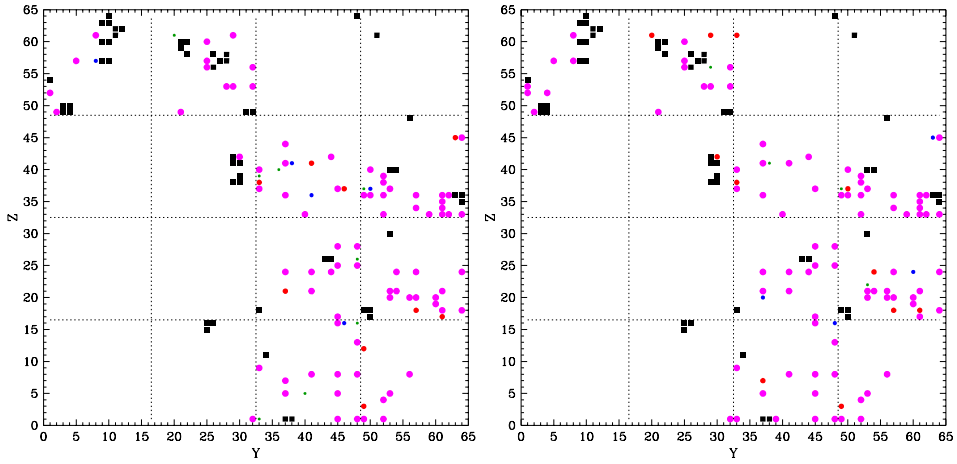

Figure 16: Distribution of "nervous" pixels on the detector plane. Left: results for $1848 - 3564$ keV, right: $3564 - 6720$ keV.

of count rate ratios obtained for a given pixel in the source and background maps. Obviously, the relevance of various background maps will be shown in the most adequate way by comparing the sky images of the source region obtained with them. However, preparation of final images is time (and disk space) consuming then the method based on shadowgrams ratios may be used to eliminate some highly inadequate background maps.

3.6 Tests with Background Maps Applied

The set of background maps was tested with the data from two staring observations of Crab from revolutions 39 and 102. The obtained image is also much less noisy when compared to the image obtained for the second background map collected in the rev. 39 closest period, i.e. map from revolution 38. Background maps from rev. 96 and "au03" showing broad ratios distributions are very bad for this observation, especially in the lowest energy band. The "long" background map allows in addition to have a clear detection in the $672 - 1036$ keV energy band.

For observation done in rev. 102 the situation is inversed, the background maps collected in the almost same time, 0096 and "au03", are better here, in particular for the first energy range. The application of

the latter map, with much longer exposure, leads to a flatter image.

The set of following Figures 17-18 presents the histograms obtained for all images presented here. It is worth interesting that the most narrow significance distribution is not always obtained for the best map. At last, to show quantitatively the detection level, a projections of significance maps along the row including pixel with the highest significance, is presented in Figures 19-20.

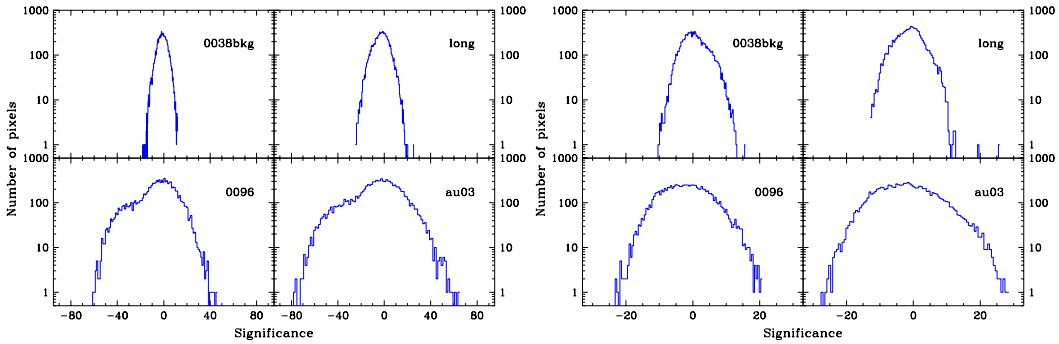

Figure 17: Significance histograms for Crab staring observation from revolution 39. Energy range: (*left*) 203 – 252 keV; (*right*) 252 – 336 keV.

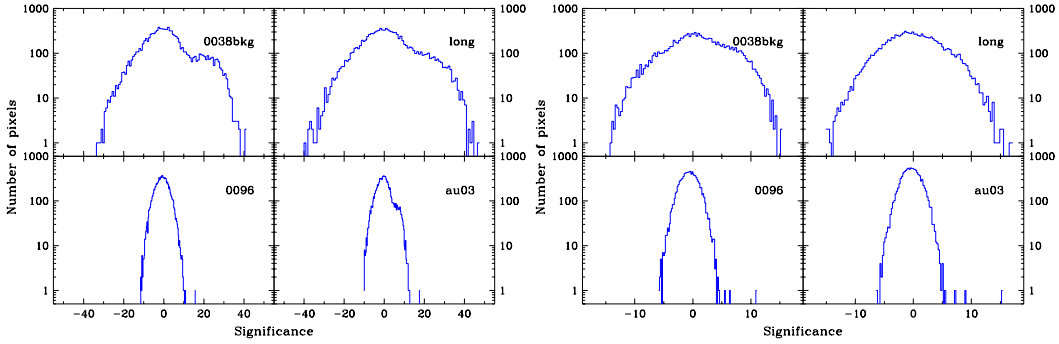

Figure 18: Significance histograms for Crab staring observation from revolution 102. Energy range: (*left*) 203 – 252 keV; (*right*) 252 – 336 keV.

4 The correction for background in OSA

Major improvements in the background maps were already present in OSA4, with the availability of one set of maps with very long (1.7 Ms) exposure based on the studies described in the previous section (`pics_sbac_bkg_0007.fits` and `pics_mbac_bkg_0008.fits`). With OSA5, more background maps, referring to different dates, are available (see Table 3), although the maps number 7 for singles and 8 for multiples should still be used as default.

These maps have been generated for a specific set of energy bands. This default set has been created to have the best source statistics, with the lowest possible contamination from background or other events, such as the cosmic–rays induced events (see Segreto et al. 2003), and the possibility to sum the maps of single and multiple events. These energy bands are shown in Table 4. It is worth noting that there was an update of the HEPI LUT during at the end of the revolution 169. The new binning table are slightly different from the previous one and led to some slight changes also in the energy bands (compare with Table 1 in the previous version of the present report). It is obvious that the user is free to select any type of energy band, but, in this case, he/she has also to built a new set of background maps.

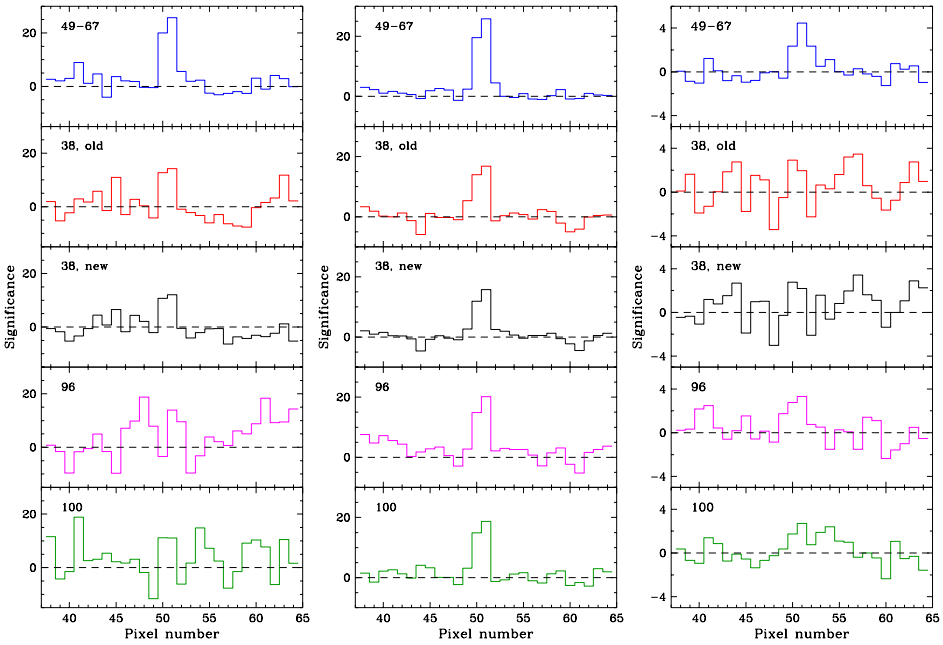

Figure 19: Horizontal projection of significance map for Crab staring observation from revolution 39. Energy range: (*left*) 203 – 252 keV; (*center*) 252 – 336 keV; (*right*) 672 – 1036 keV.

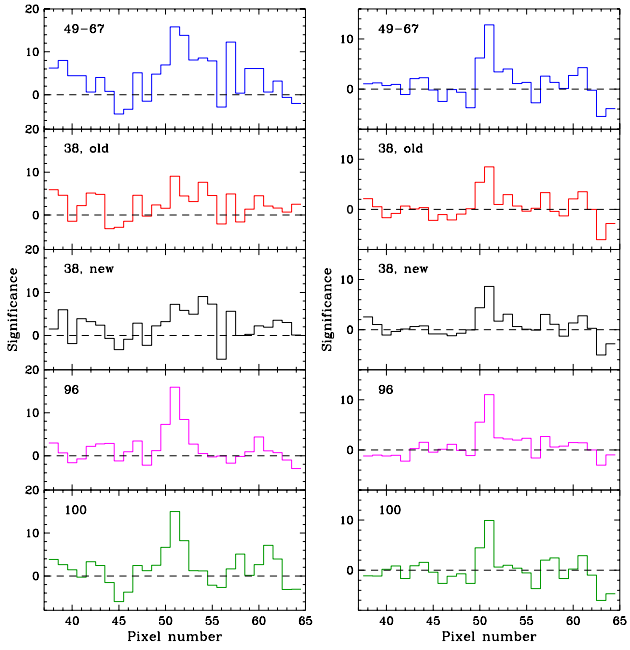

Figure 20: Horizontal projection of significance map for Crab staring observation from revolution 102. Energy range: (*left*) 203 – 252 keV; (*right*) 252 – 336 keV.

Presently the executable contains two ways to rescale the background maps: according to the time of exposure and to the average value of counts. Although a more detailed study is necessary, it appears that the average value scaling could give better results.

Table 3: Set of background maps available with OSA5. Columns: (1) Start time of integrated data [YYYY-MM-DD]; (2) Number of map set (single/multiple events); (3) Exposures (single/multiple) [Ms]; (4) Revolutions integrated.

Date (1)	Single/Multiple (2)	Exposures (3)	Revs (4)
$2003-03-09$	0007/0008	1.7/1.4	$49-67$
$2003-05-10$	0008/0009	0.94/0.93	$70-92$
$2003-08-02$	0009/0010	0.38/0.38	$97-103^*$
$2003-09-24$	0010/0011	1.4/1.4	$115-123$
$2003-12-12$	0011/0012	0.19/0.18	$142-157$
$2004-02-07$	0012/0013	1.4/1.4	$161-175$

* Without part of the revolutions 102/103 when pointing to the Crab.

Table 4: PICsIT Energy Bands. Columns: (1) Channel number in standard mode; (2) Energy [keV].

Channels Standard (1)	Energy (2)	Channels Standard (1)	Energy (2)
	Single Events		Multiple Events
$10-16$	$203-252$	$5-12$	$336-448$
$17-28$	$252-336$	$13-28$	$448-672$
$29-40$	$336-448$	$29-45$	$672-1036$
$41-56$	$448-672$	$45-74$	$1036-1848$
$57-82$	$672-1036$	$75-136$	$1848-3584$
$83-140$	$1036-1848$	$137-194$	$3584-6720$
$141-198$	$1848-3584$	$194-215$	$6720-9072$
$199-254$	$3584-6720$	$216-254$	$9072-13440$

5 Cosmic–ray induced events

Since the beginning of the in–flight operations, it was clear that there were spurious events contaminating the detector in addition to the backgroud and source events([4]). The cause was identified in cosmic–ray induced events, that are roughly the 10% of the total events and affect mainly the energy bands below 300 keV (Segreto et al. 2003, see also Natalucci 2003). As underlined by Natalucci (2003) these fake events can significanly affect the performances of PICsIT. Moreover, there are also some noisy pixels (not hot pixels, that are killed by the onboard software), but it is not well known the origin of the noise (electronics?). Anyway, the effect on the detector of these problems is the same: to produce pixels with anomalous counts (see Fig. 21).

It is possible to perform a cleaning only in photon–by–photon mode, by acting on the single count. In standard mode, since only histograms are downloaded, an *a posteriori* correction is available: when the pixel counts are higher than a constant multiplied by the average count values, i.e. $counts > k \cdot average$, the pixel value is reset to the mean value. First tests showed a certain effectiveness of this correction, although the random nature of this type of correction introduces strong fluctuations in the count rates and significances in the reconstructed sky images.

This hypothesis is confirmed by the analysis of photon–by–photon data: indeed, in this case, it was possible to develop an algorithm to delete from the photon list those events that can be identified as fake.

[4] See some nice animations by the IBIS Team in Tübingen at http://astro.uni–tuebingen.de/groups/integral/anim_gif/.

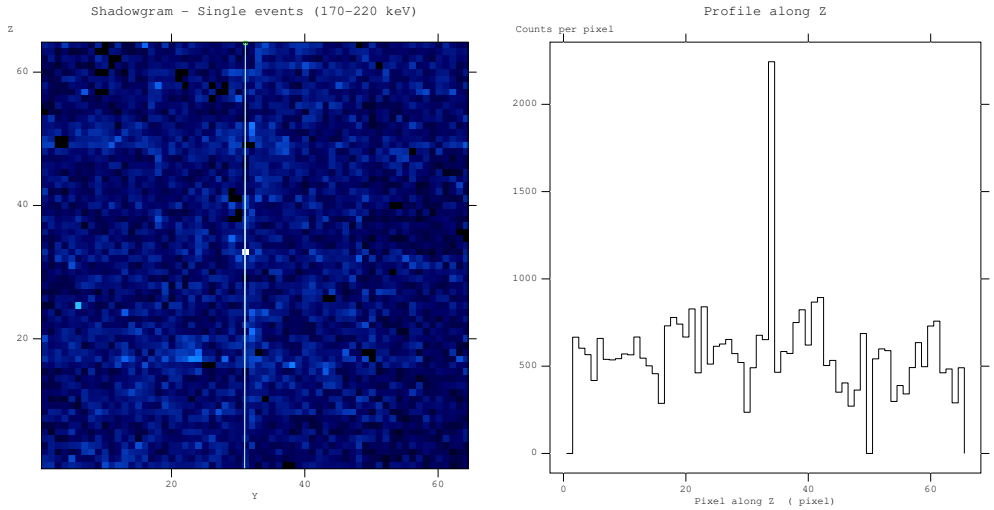

Figure 21: Effect of cosmic-rays induced events and/or noisy pixels on the shadowgrams. The white pixels have an anomalous high count value. This example is taken from the data of revolution 24 in the energy band $170 - 220$ keV; PICsIT was in photon–by–photon mode.

File Edit Tools

	DELTA_TIME 1B	PICSIT_PHA 1I	PICSIT_Y 1B	PICSIT_Z 1B
1	123	30	45	22
2	128	25	54	62
3	130	35	36	4
4	132	30	15	9
5	133	39	11	56
6	139	40	62	33
7	141	39	31	57
8	146	24	13	18
9	150	24	13	18
10	152	24	13	18
11	154	25	13	18
12	156	24	13	18
13	157	28	31	20
14	159	24	13	18
15	163	24	13	18
16	164	24	13	18
17	166	24	13	18
18	167	73	42	46
19	167	26	2	24
20	176	28	19	3

Figure 22: Identification in the photon list (single events) of fake events produced by cosmic–rays and/or noisy pixels. Spurious events are emphasized in blue.

After having isolated some of these "tracks", the photon list displayed series of photons "packed" in a very short time scale hitting a single pixel. Such "packets" are shown in Fig. 22, where fake events are emphasized in blue.

By removing these "packets" it is possible to obtain a cleaned shadowgram (Fig. 23), but – obviously – this is possible only when PICsIT is set to operate in photon–by–photon mode. Since the available telemetry is not sufficient for this type of mode, PICsIT works almost always in standard mode (i.e. with events integrated onboard in histograms). In this mode, there is no possibility to act on the single photon and, therefore, it is possible only to operate the *a posteriori* correction described above.

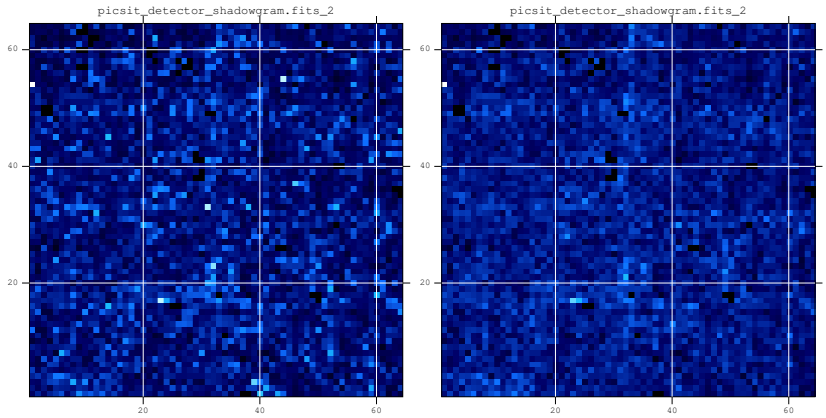

Figure 23: Effect of cosmic–rays induced events and/or noisy pixels on the shadowgrams (photon–by–photon mode). (*left*) Normal shadowgram; (*right*) Cleaned shadowgram. After the cleaning, the bright pixels disappeared. The only bright pixel remained at the top left of the cleaned shadowgram is a well–known pixel that often is hot. Data from revolution 14, energy band $170 - 250$ keV.

At the time of updating the present report, a study to remove these fake events onboard has been presented (Labanti et al. 2005). In this case, the cleaning would be performed on board before to integrate the histogram, so that the downloaded histogram would be cleaned from the cosmic-rays induced events. A set of observations of the Crab and an empty field in photon-by-photon mode have been performed in March 2005 (Rev. 300), to test the effectiveness of the proposed solution. Preliminary results show an increase of sensitivity below 250 keV by a factor of ~ 2, as expected. A more detailed study is ongoing.

6 The sky image reconstruction

Here are shown some performances of the PICsIT ISSW. Details on the techniques of the deconvolution are available in Goldwurm et al. (2003).

6.1 Sky coordinates reconstruction

The sensitivity of PICsIT does not allow to see sources during a typical exposure of one ScW (2 ks), but there are sometimes Scw with duration of 5 ks. In this case, there is the possibility to detect the Crab at level of $SNR = 3 - 4\sigma$. During the observations of calibration performed in February 2003, the Crab was pointed during the revolutions 39, 43, 44, and 45 (staring and dithering hexagonal and 5×5). The coordinates of the Crab detected at $SNR > 3\sigma$ are reported in the Fig. 24. All the positions are within an error of $\pm 5'$ from the catalog position.

6.2 Image analysis

For the analysis with the Crab were selected the data obtained in February 2003 and the results are shown in the Table 5. The tests on the previous versions of OSA (3 and 4) have been run on the data of the Rev. 39, where the Crab was on axis and the satellite was staring on the target. The observation was about 102 ks long, but by using only the complete histograms, the effective exposure is reduced to 77 ks. The OSA4 tests were divided into two parts: (I) by integrating all the ScW shadowgrams before the deconvolution with `sumhist` module and (II) by deconvolving the shadowgrams every Scw and then

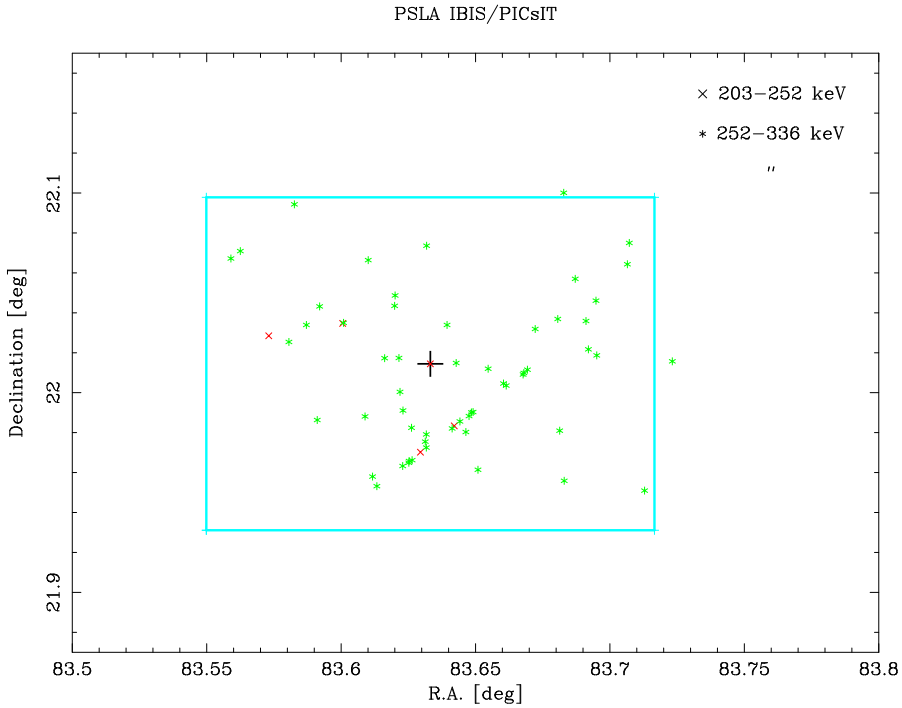

Figure 24: Sky coordinate reconstruction of the Crab position obtained with the ScW detections with $SNR > 3\sigma$ (Exposure 5 ks) in the energy band $252 - 336$ keV (*) and $203 - 252$ keV ($\times$). The catalog position of the Crab is shown at the centre of the figure and indicated with +. The surrounding square represents the pixel of PICsIT with $10'$ size.

Table 5: PICsIT observations of the Crab with different OSA versions. See the text for detailed explanations. Please note that OSA3 had slightly different energy bands, but the effect on the SNR and count rate is negligible. The change in count rates in OSA5 are mainly due to a revision of the deconvolution algorithm.

	OSA3		OSA4 I		OSA4 II		OSA5	
Energy Band (keV)	Rate (c/s)	SNR (σ)	Rate (c/s)	SNR (σ)	Rate (c/s)	SNR (σ)	Rate (c/s)	SNR (σ)
$203 - 252$	2.5	7.4	3.0	23.9	3.0	23.9	1.50	51
$252 - 336$	2.2	11.0	2.5	23.6	2.5	23.6	1.71	115
$336 - 448$	1.3	7.1	1.2	13.7	1.2	13.7	0.75	58
$448 - 672$	0.7	4.4	0.7	7.6	0.7	7.6	0.49	36
$672 - 1036$	–	–	0.3	4.2	0.3	4.2	0.18	12

summing them later with `ip_skymosaic`. Being the deconvolution a linear operation, the results should be equal, as it is (at least within the first decimal digit).

Tests on OSA5 have been done by using all the Crab observation in February 2003 (Revs $39 - 45$), with PICsIT in standard mode, for a total of 677 ks of exposure. The Crab was observed in different positions in the FOV and up to 12.5° from the centre[5]. The values reported here are obtained with `ip_skyimage` set to use the variance shadowgrams not corrected and to generate the variance maps in output in order

[5]Indeed, starting from OSA5 it is possible to deconvolve the whole FOV ($\approx 29° \times 29°$). In the past versions, before the availability of the OSA4 background maps, the deconvolved FOV of PICsIT was reduced to about ($\approx 16° \times 16°$) to avoid the borders of the partially-coded FOV that were extremely noisy.

to use and test the `varmosaic` tool of `HEASoft`. The `ip_skymosaic` module provides similar results. Since the variance shadowgrams are not corrected, the removal of residual artifacts and background in the significance maps is done in the usual way, i.e. by studying the SNR distribution in the significance maps.

The best performances of PICsIT are obtained with long background maps in the energy band 252 – 336 keV, that is less affected by the cosmic–rays induced events and is in a range sufficiently low to detect enough photons. In the Fig. 25 is shown how the availability of good long background maps improved significantly the detection of the Crab.

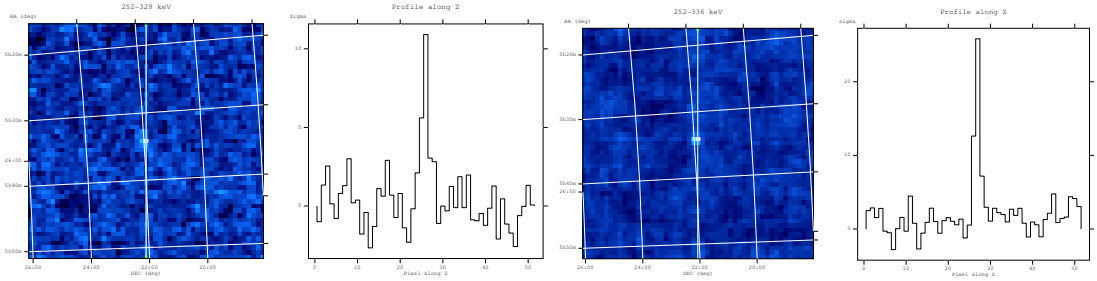

Figure 25: (*left*) Crab observation during the rev 39 (staring, on axis, 77 ks). Significance map and profile in the energy band 252 – 329 keV. (*right*) The same as above, but with OSA4.

The greatest differences in the count rates and significance (for observations in staring, dithering, off axis) occur just the band 203 – 252 keV, where we expect that the impact of cosmic–ray induced events is still high and the *a posteriori* correction – the only available since PICsIT is operated in histogram mode – may not be too much accurate (see Sect. 5).

The study of the whole data set of Crab observations (Revs. 39 – 45, Revs. 102 – 103, Rev. 170, Rev. 239) evidenced two problems yet to be solved. The first refers to the presence of some Scw with problems in attitude data: in this case, the software read the pointing coordinates from keywords in the ScW group, but these values are not corrected for instruments misalignement. This can generate an offset in the position of about $9'$ ($\approx$ 1 PICsIT pixel), and therefore can reduce the SNR of the mosaic image.

The second problem is an offaxis effect: as the source is placed at the edges of the FOV, the SNR decreases significantly. Therefore, when looking at the data in Table 5, these two problems should be taken into account. A correction will be soon available in the forthcoming versions of OSA.

It is worth mentioning that during the observations of the calibration sources some tests of the photon-by-photon mode have been set up and performed, with special telemetry allocation to PICsIT (e.g. revolutions 39 and 40). However, despite this configuration, the limited telemetry budget resulted in a loss of about 80% of the pointing time. From an observation 100 ks long at the beginning of the revolution 40, the effective exposure is only 23 ks. An inspection of the GTI table and of the lightcurve revealed that the missing time was due to telemetry gaps.

7 Spectra

With OSA 4.2, the first set of RMF/ARF files have been released and are not changed in OSA5. Only the files for single events are scientifically useful, while the corresponding files for multiples are dummy.

Two ways are presently available to extract single sources spectra from PICsIT data: the first, and also the more reliable and stable, uses the count rates and errors obtained from the imaging pipeline. That is, OSA for PICsIT is run up to IMA2 level, then the mosaic is done, and the detected source count rate

and error are read from the intensity and significance maps. M. Chernyakova (ISDC) has also prepared a Perl script to make these operations automatic[6]. An example of the Crab spectrum is shown in Fig. 26. The PICsIT data have been obtained from the integration of all the data in standard mode from the Crab observations in February 2003 (see Table 5) and are fit with 5% of systematics. The intercalibration constant between ISGRI (set as reference) and PICsIT is 0.64 ± 0.05.

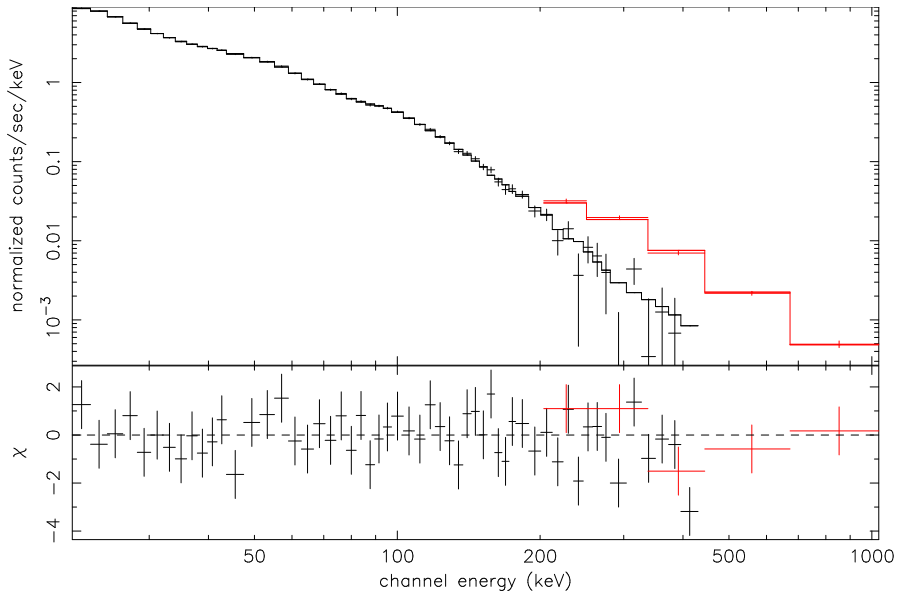

Figure 26: IBIS (ISGRI+PICsIT) spectrum of the Crab. Data of ISGRI are from rev. 102, while data of PICsIT are from the standard mode Scw in the revs. $39 - 45$.

The other way is to run the pipeline from BIN_S to SPE level, thus using the `ip_spectra_extraction` module. However, since PICsIT sources are very faint in a high background[7] and results are not yet satisfactory. An alternative solution is currently under study.

Presently, it is better to use the first way (imaging) – although limited by the availability of background maps – that gives the best reliable results. A clear example is presented in Cadolle-Bel et al. (2005), where the spectrum of Cyg X-1 is presented, together with the other instruments.

8 Timing

In February 2003, during the observation of the Crab, IBIS/PICsIT was set up to test the timing performances in the different modes of operation, i.e. photon–by–photon and spectral timing. For the moment, in the OSA, it is available the possibility to build the lightcurve for the whole detector with the spectral timing data. Therefore, we report here some tests on this part of the software.

The data analysed are from the revolutions 40 and 41, with PICsIT set up in spectral timing with 1 ms time resolution and 4 energy bands ($156 - 208$, $208 - 260$, $260 - 364$, $364 - 676$ keV). The total exposure was 310 ks.

The data in output from the pipeline were corrected for barycenter with `barycent` tool of OSA. The

[6]The script is publicly available at `http://isdc.unige.ch/index.cgi?Soft+scripts`.

[7]It is worth reminding that the Crab has a count rate of less than 10 c/s over the whole energy range for single events, to be compared with a background of about 2500 c/s.

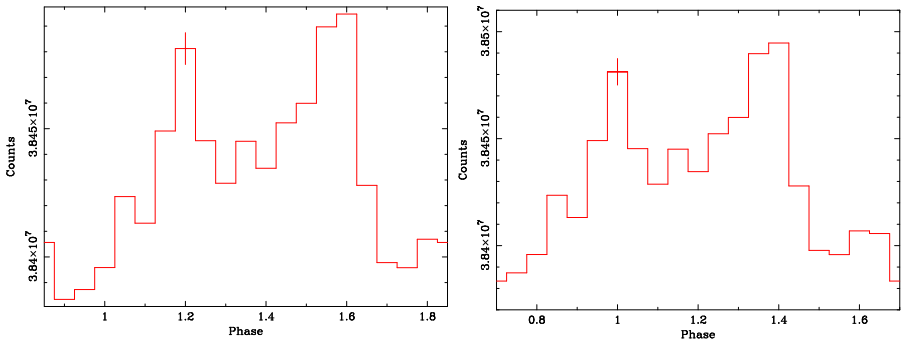

Figure 27: (*left*) Crab observation during the rev $40-41$ (spectral timing, 1 ms time resolution). Folded lightcurve in the energy band $260-364$ keV. (*right*) The same as above, but manually aligned to the known Crab phase.

folded lightcurve shows a shift in the phase of ≈ 0.2 (6 ms for the Crab) (Fig. 27, *left*). This, for the moment, should be corrected manually (Fig. 27, *right*).

Starting from Rev. 294 the spectral timing mode has been set to this new values: 4 energy bands ($260-364$, $364-676$, $676-1196$, $1196-2600$ keV) with 4 ms of time resolution, in order to explore the MeV energy range. This could be useful particularly in studies of GRB, coordinated with Compton mode, since PICsIT is the only instrument presently available, able to reach the MeV energy range.

9 Known problems in OSA for PICsIT and things to do

Presently, these were the problem known in the OSA5.1 for PICsIT:

1. An improvement in the PICsIT spectrum extraction executable with the PIF method has been implemented in the OSA 5.1. Despite the improvement under certain conditions (e.g. staring observations), the algorithm is still unstable. We still suggest the user to continue adopting the spectra extraction from images, as explained in OSA4.2. A RMF already rebinned for the channels of the imaging pipeline is available in the IC files.
2. Phase shift in spectral timing mode.

Major improvements to be added in OSA for PICsIT are: mask transparency, PIF calculation for off-axis sources, improvement of background subtraction for very long mosaics, full use of multiple events.

10 Final remarks

Further informations, presentations, reports on PICsIT, together with the catalog of the sources detected to date, are available at the IBIS/PICsIT web page at INAF/IASF-Bologna, created and maintained by F. Schiavone:

`http://www.iasf-bologna.inaf.it/Research/INTEGRAL/`

11 References

- Cadolle Bel M., Sizun P., Goldwurm A., et al., 2005, A&A, accepted for publication (`astro-ph/0509851`).
- Calabretta M.R., Greisen E.W., 2002, A&A 395, 1077
- Courvoisier T.J.-L., Beckmann V., Bourban G., et a., 2003, A&A 411, L343
- Di Cocco G., Caroli E., Celesti E., et al., 2003, A&A 411, L189
- Ebisawa K., Bourban G., Bodaghee A., et al., 2003, A&A 411, L59
- Ferguson C., Barlow E.J., Bird A.J., et al., 2003, A&A 411, L19
- Goldwurm A., Goldoni P., Gros A., et al., 2001, In: "Exploring the gamma–ray universe. Proceedings of the Fourth INTEGRAL Workshop", 4-8 September 2000, Alicante, Spain. Editor: B. Battrick, Scientific editors: A. Gimenez, V. Reglero, and C. Winkler. ESA SP–459, p. 497.
- Goldwurm A., David P., Foschini L., et al., 2003, A&A 411, L223
- Labanti C., Di Cocco G., Marisaldi M., et al., "Proposal for recovering PICsIT low energy range", March 2005.
- Laurent P., Limousin O., Cadolle Bel M., et al., 2003, A&A 411, L185
- Malaguti G., Bazzano A., Bird A.J., et al., 2003, A&A 411, L173
- Natalucci L., Bird A.J., Bazzano A., et al., 2003, A&A 411, L209
- Segreto A., Labanti C., Bazzano A., et al., 2003, A&A 411, L215